Atmos. Meas. Tech., 3, 209–232, 2010
www.atmos-meas-tech.net/3/209/2010/

Atmospheric Measurement Techniques

A method for improved SCIAMACHY CO_2 retrieval in the presence of optically thin clouds

M. Reuter, M. Buchwitz, O. Schneising, J. Heymann, H. Bovensmann, and J. P. Burrows

University of Bremen, Institute of Environmental Physics, P.O. Box 330440,
28334 Bremen, Germany

Received: 28 August 2009 – Published in Atmos. Meas. Tech. Discuss.: 8 October 2009
Revised: 15 January 2010 – Accepted: 9 February 2010 – Published: 12 February 2010

Abstract. An optimal estimation based retrieval scheme for satellite based retrievals of XCO_2 (the dry air column averaged mixing ratio of atmospheric CO_2) is presented enabling accurate retrievals also in the presence of thin clouds. The proposed method is designed to analyze near-infrared nadir measurements of the SCIAMACHY instrument in the CO_2 absorption band at 1580 nm and in the O_2-A absorption band at around 760 nm. The algorithm accounts for scattering in an optically thin cirrus cloud layer and at aerosols of a default profile. The scattering information is mainly obtained from the O_2-A band and a merged fit windows approach enables the transfer of information between the O_2-A and the CO_2 band. Via the optimal estimation technique, the algorithm is able to account for a priori information to further constrain the inversion. Test scenarios of simulated SCIAMACHY sun-normalized radiance measurements are analyzed in order to specify the quality of the proposed method. In contrast to existing algorithms for SCIAMACHY retrievals, the systematic errors due to cirrus clouds with optical thicknesses up to 1.0 are reduced to values below 4 ppm for most of the analyzed scenarios. This shows that the proposed method has the potential to reduce uncertainties of SCIAMACHY retrieved XCO_2 making this data product potentially useful for surface flux inverse modeling.

1 Introduction

CO_2 is the dominant anthropogenic greenhouse gas but there are still large uncertainties of its natural global sources and sinks (Stephens et al., 2007). Global measurements of the atmospheric CO_2 concentration can be used as input for inverse models to reduce these uncertainties. In-situ CO_2 measurements of networks such as the NOAA (National Oceanic and Atmospheric Administration) carbon cycle greenhouse gas cooperative air sampling network (http://www.esrl.noaa.gov/gmd/ccgg/flask.html) are very accurate. However, the sparseness of the measurement sites and their world wide distribution with a majority over US and European land surfaces and a minority on the Southern Hemisphere limit the current knowledge of CO_2 surface fluxes. Theoretical studies have shown that satellite measurements of CO_2 have the potential to significantly reduce the surface flux uncertainties. This requires a precision of about 1% for regional averages and monthly means (Rayner and O'Brien, 2001; Houweling et al., 2004). However, undetected biases of a few tenths of a part per million on regional scales can already hamper inverse surface flux modeling (Miller et al., 2007; Chevallier et al., 2007).

Currently, there are only a few satellite instruments in orbit which are able to measure atmospheric CO_2. The High Resolution Infrared Radiation Sounder (HIRS) (Chédin et al., 2002, 2003), the Atmospheric InfraRed Sounder (AIRS) (Engelen et al., 2004; Engelen and McNally, 2005; Aumann et al., 2005; Strow et al., 2006; Maddy et al., 2008), and the Infrared Atmospheric Sounding Interferometer (IASI) (Crevoisier et al., 2009) perform CO_2 sensitive measurements in the thermal infrared (TIR) spectral region, i.e. these instruments do not detect reflected solar radiation but thermal radiation emitted from surface and atmosphere. This brings the advantage that measurements are possible not only at day-time but also at night-time. However, the disadvantage of such measurements is their lack of sensitivity in the lower troposphere where the strongest signals due to sources and sinks can be expected.

In contrast to this, the sensitivity of instruments measuring reflected solar radiation in the near-infrared (NIR)/shortwave infrared (SWIR) spectral region is much more constant

Correspondence to: M. Reuter
(maximilian.reuter@iup.physik.uni-bremen.de)

(with height) and shows maximum values near the surface, typically. Note that in this paper NIR and SWIR are commonly referred to as NIR. At present, SCIAMACHY aboard ENVISAT launched in 2002 (Bovensmann et al., 1999) and TANSO (Thermal And Near infrared Sensor for carbon Observation) aboard GOSAT (Greenhouse gases Observing SATellite) launched in 2009 (Yokota et al., 2004) are the only orbiting instruments measuring NIR radiation in appropriate absorption bands at around 0.76, 1.6, and 2.0 µm with sufficient spectral resolution to retrieve XCO_2. Another carbon dioxide observing satellite was OCO (Orbiting Carbon Observatory) (Crisp et al., 2004). OCO was designed to measure within the same spectral region. Unfortunately, the satellite was lost shortly after lift-off on 24 February 2009 (Palmer and Rayner, 2009).

Contrary to TANSO, SCIAMACHY was not especially designed for the retrieval of XCO_2 with the precision and accuracy needed to enhance our knowledge about sources and sinks via inverse modeling. Due to SCIAMACHY's lower spatial and spectral resolution, the achievable accuracy and precision is expected to be lower compared to a TANSO like instrument. Nevertheless, within the time period 2002–2009 SCIAMACHY was the only instrument measuring XCO_2 from space with significant sensitivity also to the lower troposphere. Therefore, the development of algorithms deriving XCO_2 from SCIAMACHY as accurate as possible with realistic error estimates is crucial to start a consistent long-term time series of XCO_2 observations from space.

In the literature one can find several somewhat different XCO_2 retrieval algorithms for SCIAMACHY data: The WFM-DOAS algorithm (Weighting Function Modified Differential Optical Absorption Spectroscopy) was developed at the University of Bremen for the retrieval of trace gases from SCIAMACHY and has been described by Schneising et al. (2008), Buchwitz et al. (2005a,b, 2000b), and Buchwitz and Burrows (2004). This algorithm is based on a fast look-up table (LUT) based forward model used to derive the number of CO_2 and O_2 molecules in the atmospheric column in order to derive XCO_2. Other groups have developed somewhat different approaches to retrieve XCO_2 or CO_2 columns from SCIAMACHY. The computationally much more expensive FSI/WFM-DOAS algorithm (Full Spectral Initiation WFM-DOAS) described by (Barkley et al., 2006a,c,b, 2007) derives XCO_2 by retrieving the number of CO_2 molecules from SCIAMACHY but determining the air column from meteorological analysis of the surface pressure. This applies also to the algorithm discussed by Houweling et al. (2005). The retrieval algorithm designed for OCO follows the strategy to determine XCO_2 from column measurements of CO_2 and simultaneous measurements of the surface pressure derived from measurements in the O_2-A band (Connor et al., 2008). Bösch et al. (2006) applied a modified version of this algorithm with a reduced number of state vector elements to SCIAMACHY data in a surrounding of the Park Falls FTS-site. As SCIAMACHY's channel 7 suffers from a light-leak and ice on the detector, all these algorithms derive the number of CO_2 molecules from the weak CO_2 absorption band at around 1.6 µm and not from the much stronger band at around 2.0 µm. Bösch et al. (2006) and Schneising et al. (2008) showed that XCO_2 can be retrieved from SCIAMACHY with a single measurement precision of 1–2% assuming clear sky conditions. Additionally, Schneising et al. (2008) showed that a relative accuracy of about 1–2% for monthly averages at a spatial resolution of about $7^\circ \times 7^\circ$ can be achieved from SCIAMACHY measurements under clear sky conditions.

However, scattering at aerosol and/or cloud particles remains a major source of uncertainty for SCIAMACHY XCO_2 retrievals which easily exceeds the precisions and accuracy estimated for clear sky conditions. Houweling et al. (2005) found that the XCO_2 retrieval error may amount to 10% in the presence of mineral dust aerosols. Schneising et al. (2008) showed that a thin scattering layer with an optical thickness of 0.03 in the upper troposphere can introduce XCO_2 uncertainties of up to several percent. They derived a XCO_2 error of 8.80% resulting from a CO_2 column error of -0.89% and a O_2 column error of -8.91% for a scenario with an albedo of 0.1. Aben et al. (2007) found an underestimation of space-based measurements of the CO_2 column of 8% for a scenario with a cirrus cloud optical thickness (COT) of 0.05 and a surface albedo of 0.05. The underestimation amounted to 1% for an albedo of 0.5.

Unfortunately, thin clouds with optical thicknesses below 0.1 cannot easily be detected within nadir measurements in the visible and near infrared spectral region (e.g. Reuter et al., 2009; Rodriguez et al., 2007).

Satellite occultation measurements as well as lidar observations show that sub visible cirrus clouds occur quite frequently with a maximum occurrence probability of about 45% within the tropics, seasonally following the inter tropical convergence zone (ITCZ) (Wang et al., 1996; Winker and Trepte, 1998; Nazaryan et al., 2008). The WFM-DOAS 1.0 XCO_2 retrieval for SCIAMACHY has a low quality over dark ocean surfaces and is therefore applied to land surfaces only. The global distribution of the continents shows that the land masses of the Southern Hemisphere are closer to the equator. For this reason, southern hemispheric SCIAMACHY XCO_2 retrievals are statistically much more affected by undetected sub visible cirrus clouds compared to northern hemispheric retrievals. Analyzing data of the lidar instrument CALIOP (Cloud-Aerosol LIdar with Orthogonal Polarization) aboard the CALIPSO satellite (Cloud-Aerosol Lidar and Infrared Pathfinder Satellite Observations), Schneising et al. (2008) found that discrepancies of the southern hemispheric annual cycle of SCIAMACHY retrieved XCO_2 and corresponding values of NOAA's CO_2 assimilation system CarbonTracker (Peters et al., 2007) can be most likely explained by sub visible cirrus clouds.

Having in focus the spectrally high resolving satellite instruments TANSO aboard GOSAT and OCO, algorithms have been developed to correct for scattering effects. Bril et al. (2007) developed a method which is based on application of the equivalence theorem and photon path-length statistics with further parameterization of the photon path-length probability density function (PPDF) for a TANSO like instrument. They derive effective scattering parameters of cirrus clouds and aerosols from the O_2-A band and from saturated water vapor lines at around 2.0 µm. This information is used to correct the CO_2 retrieval in the 1.6 µm CO_2 band. Kuang et al. (2002) proposed a method based on simultaneously fitting cloud and aerosol parameters (and others) within the three spectral bands of OCO at around 0.76, 1.6, and 2.0 µm. They estimated that a precision of 0.3 to 2.5 ppm is achievable for aerosol optical thicknesses (AOT) of up to 0.3.

In contrast to both methods, the XCO_2 retrieval algorithms for SCIAMACHY mentioned above do not explicitly account for scattering effects. They either do not account for scattering at all or in an indirect way as the WFM-DOAS algorithm does by assuming that photon path-length modifications are identical at 0.76 and 1.6 µm. In this approximation, scattering errors of CO_2 and O_2 cancel out when calculating XCO_2.

Within the publication at hand, a new XCO_2 retrieval algorithm optimized for SCIAMACHY nadir data is introduced explicitly considering scattering in an (optically thin) ice cloud layer and at aerosols of a default profile. The physical basis for simultaneously retrieving scattering related parameters and XCO_2 using a merged fit windows approach is described in Sect. 2. The information about these scattering parameters comes mainly from the measurements in the O_2 fit window. The usability of SCIAMACHY or GOME measurements in this spectral region for the retrieval of cloud parameters is already confirmed within several publications (e.g. Kokhanovsky et al., 2006; Wang et al., 2008; van Diedenhoven et al., 2007). Section 3 describes the inversion technique based on optimal estimation. Within this section, details of the forward operator, the state vector, and the usage of prior knowledge is discussed. An error analysis is given in Sect. 4. Here, the retrieval algorithm is applied to simulated SCIAMACHY data in order to specify the algorithm's sensitivity to the state vector elements but also to parameters that are not retrieved within the state vector. In this regard, special emphasis is put on cloud parameters which are not retrieved.

2 Physical basis

The WFM-DOAS algorithm (Schneising et al., 2008; Buchwitz et al., 2005a,b, 2000b; Buchwitz and Burrows, 2004) retrieves several independent parameters from SCIAMACHY measurements in the spectral region dominated by CO_2 absorption from 1558 to 1594 nm (in the following referred to as the "CO_2 fit window") and also from measurements in the spectral region of the O_2-A band from 755 to 775 nm (in the following referred to as the "O_2 fit window"). Within the CO_2 fit window the number of CO_2 molecules, the number of H_2O molecules, the atmospheric temperature, spectral shift and squeeze, and a 2nd order polynomial are retrieved. The number of CO_2 molecules is retrieved by shifting a reference profile with constant mixing ratio. In the same manner, the number of H_2O molecules as well as the atmospheric temperature is determined by shifting reference profiles. Separately from this, the number of O_2 molecules, the atmospheric temperature, spectral shift and squeeze, and a 2nd order polynomial are retrieved in an analogous way from the O_2 fit window. Beforehand, an albedo retrieval is performed in both fit windows using measurements in micro windows (nearly) without absorptions line features at the edge of both fit windows.

Each of these parameters influences the spectrum of reflected solar radiation measured at the satellite instrument. The partial derivatives of the measured radiation with respect to a parameter is called the weighting function (or Jacobian) of this parameter. Of course, it is only possible to retrieve those parameters having a unique weighting function, sufficiently different from all other weighting functions in terms of the instrument's precision. Very similar weighting functions can result in ambiguities of the retrieved corresponding parameters.

Figure 1 shows for exemplary atmospheric conditions with moderate aerosol load and one thin ice cloud layer the weighting functions of three different scattering related parameters under a typical observation geometry in SCIAMACHY's spectral resolution. Additionally, the figure shows the XCO_2 weighting function which gives the change of radiation when columnar increasing the CO_2 concentration by 1 ppm. For this example, the magnitude of its spectral signature is comparable to a change of the cloud top height (CTH) by 1 km, the cloud water/ice path (CWP) by 0.2 g/m^2, or to a change of the aerosol load by 100%. It is immediately noticeable that there are high correlations between the curves. Especially between the aerosol profile scaling (APS) and the cloud water/ice path weighting function as well as between the cloud top height and the XCO_2 weighting function.

XCO_2 changes of 1 ppm are approximately the detection limit due to SCIAMACHY's signal to noise (SNR) characteristics. This means, with SCIAMACHY it is actually not possible to discriminate XCO_2 values of a few ppm from changes of the given scattering parameters. For example, decreasing the cloud top height from 14 to 10 km spectrally changes the radiation in (nearly) the same way as increasing XCO_2 by 4 ppm does. Most likely, it is not possible to retrieve scattering parameters simultaneously with the number of CO_2 molecules, i.e. uncertainties of the scattering parameters will always result in uncertainties of the retrieved CO_2 molecules when solely analyzing measurements from the CO_2 fit window.

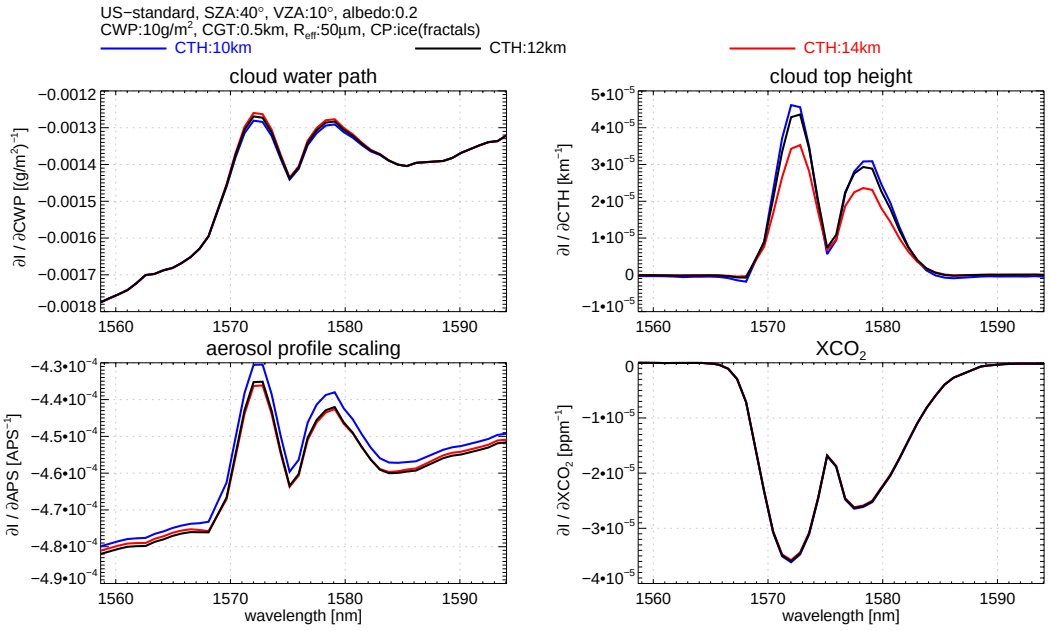

Fig. 1. Weighting functions in the CO_2 fit window for three cloud scenarios based on a US-standard atmosphere including an optically thin ice cloud with a cloud top height of 10 km (blue), 12 km (black), and 14 km (red): cloud water/ice path (top/left), cloud top height (top/right), scaling of the aerosol profile (bottom/left), and XCO_2 (bottom/right). The weighting functions are calculated with the SCIATRAN 3.0 radiative transfer code and are folded with SCIAMACHY's slit function.

Analogous to Fig. 1, Fig. 2 shows for identical atmospheric conditions the weighting functions of the same scattering parameters but for the O_2 fit window. Additionally, it shows the weighting function in respect to surface pressure p_s which can be used to derive the total number of air molecules within the atmospheric column by applying the hydrostatic assumption. The similarities between the weighting functions are less pronounced in this fit window. This applies especially when comparing the surface pressure weighting function to the weighting functions of the given scattering parameters. This originates by much stronger absorption lines in this fit window. As width and depth of absorption lines depend on the ambient pressure, saturation effects differ much stronger with height within this spectral region. Additionally, SCIAMACHY's resolution resolves the spectral structures of the gaseous absorption better within this fit window. Nevertheless, there are still similarities that are not negligible e.g. between the cloud top height and aerosol profile scaling weighting function. Differences of 1 hPa are in the order of the detection limit according to SCIAMACHY's SNR characteristics. Therefore, it can be expected that independent information on the given scattering parameters can be extracted from this fit window simultaneously with information about the surface pressure.

The large differences of the three illustrated cloud top height weighting functions show that the radiative transfer can become non-linear in respect to this parameter. Additionally, the spectral similarity of the CTH and the CWP weighting function strongly depend on the scenario (large differences for the cloud at 12 km, minor differences for the cloud at 10 km). This means, depending on the individual scene, ambiguities may be more or less pronounced. In this context, also the selected surface albedo has strong influence.

In the following section we will describe, how the information on scattering parameters, which can be derived from the O_2 fit window, can be transported to the CO_2 fit window.

3 Inversion via optimal estimation

We use an optimal estimation based inversion technique to find the most probable atmospheric state given a SCIAMACHY measurement and some prior knowledge. Nearly all mathematical expressions given in this publication as well as their derivation and notation can be found in the text book of Rodgers (2000). A list of all used symbols is given by Table 1.

The forward model $\boldsymbol{F}$ is a vector function which calculates for a given (atmospheric) state simulated measurements i.e. simulated SCIAMACHY spectra. The input for the forward model are the state vector $\boldsymbol{x}$ and the parameter vector $\boldsymbol{b}$. The state vector consists of all unknown variables that shall be retrieved from the measurement (e.g. CO_2). Parameters which are assumed to be exactly known but affecting the radiative transfer (e.g. viewing geometry) are the elements of the parameter vector. The entire list of state vector elements

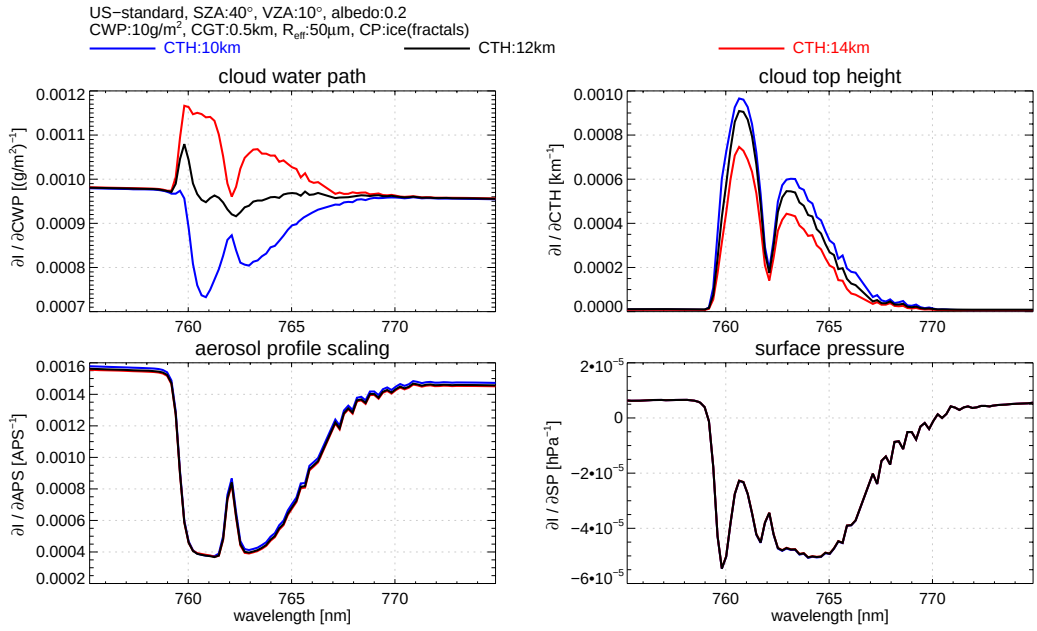

Fig. 2. Weighting functions in the O_2 fit window for three cloud scenarios based on a US-standard atmosphere including an optically thin ice cloud with a cloud top height of 10 km (blue), 12 km (black), and 14 km (red): cloud water/ice path (top/left), cloud top height (top/right), scaling of the aerosol profile (bottom/left), and surface pressure (bottom/right). The weighting functions are calculated with the SCIATRAN 3.0 radiative transfer code and are folded with SCIAMACHY's slit function.

is given in the first column of Table 3. The measurement vector $\boldsymbol{y}$ consists of SCIAMACHY sun-normalized radiances of two merged fit windows concatenating the measurements in the CO_2 and O_2 fit window. The difference of measurement and corresponding simulation by the forward model is given by the error vector $\boldsymbol{\varepsilon}$ comprising inaccuracies of the instrument and of the forward model:

$$\boldsymbol{y} = \boldsymbol{F}(\boldsymbol{x},\boldsymbol{b}) + \boldsymbol{\varepsilon} \tag{1}$$

According to Eq. (5.3) of Rodgers (2000), we aim to find the state vector $\boldsymbol{x}$ which minimizes the cost function χ^2:

$$\chi^2 = (\boldsymbol{y}-\boldsymbol{F}(\boldsymbol{x},\boldsymbol{b}))^T \mathbf{S}_\epsilon^{-1}(\boldsymbol{y}-\boldsymbol{F}(\boldsymbol{x},\boldsymbol{b})) + (\boldsymbol{x}-\boldsymbol{x}_a)^T \mathbf{S}_a^{-1}(\boldsymbol{x}-\boldsymbol{x}_a) \tag{2}$$

Here, $\mathbf{S}_\epsilon$ is the error covariance matrix corresponding to the measurement vector, $\boldsymbol{x}_a$ is the a priori state vector which holds the prior knowledge about the state vector elements and $\mathbf{S}_a$ is the corresponding a priori error covariance matrix which specifies the uncertainties of the a priori state vector elements as well as their cross correlations.

Even though the number of state vector elements (26) is smaller than the number of measurement vector elements (134), the inversion problem is generally under-determined. The weighting functions of some state vector elements show quite large correlations under certain conditions. This especially applies to the weighting functions corresponding to the ten-layered CO_2 profile but also to some of the weighting functions shown in Figs. 1 and 2. For this reason we use a priori knowledge further constraining the problem and making it well-posed. However, for most of the state vector elements the used a priori knowledge gives only a weak constraint and is therefore not dominating the retrieval results. Furthermore, we use only static (i.e. spatially and temporally invariant) a priori knowledge of XCO_2.

According to Eq. (5.8) of Rodgers (2000), we use a Gauss-Newton method to iteratively find the state vector $\hat{\boldsymbol{x}}$ which minimizes the cost function.

$$\boldsymbol{x}_{i+1} = \boldsymbol{x}_i + \hat{\mathbf{S}}[\mathbf{K}_i^T \mathbf{S}_\epsilon^{-1}(\boldsymbol{y}-\boldsymbol{F}(\boldsymbol{x}_i,\boldsymbol{b})) - \mathbf{S}_a^{-1}(\boldsymbol{x}_i-\boldsymbol{x}_a)] \tag{3}$$

$$\hat{\mathbf{S}} = (\mathbf{K}_i^T \mathbf{S}_\epsilon^{-1}\mathbf{K}_i + \mathbf{S}_a^{-1})^{-1} \tag{4}$$

Within this equation, $\mathbf{K}$ is the Jacobian or weighting function matrix consisting of the derivatives of the forward model in respect to the state vector elements $\mathbf{K}=\partial\boldsymbol{F}(\boldsymbol{x},\boldsymbol{b}))/\partial\boldsymbol{x}$. In the case of convergence, $\boldsymbol{x}_{i+1}$ is the most probable solution given the measurement and the prior knowledge and is then denoted as maximum a posteriori solution $\hat{\boldsymbol{x}}$ of the inverse problem. $\hat{\mathbf{S}}$ is the corresponding covariance matrix consisting of the variances of the retried state vector elements and their correlations.

The iteration starts with the first guess state vector $\boldsymbol{x}_0$. Often, $\boldsymbol{x}_0$ is set to $\boldsymbol{x}_a$, even though this is mathematically not mandatory and also not done here for some state vector elements. Referring to Eq. (5.29) of Rodgers (2000),

Table 1. List of used symbols and corresponding dimensions and short descriptions.

Symbol	Dimension	Description
α_λ	1	Albedo (wavelength dependent)
$\mathbf{A}$	$n \times n$	Averaging kernel matrix
$\boldsymbol{b}$	$n_b \times 1$	Parameter vector
d_l	1	Degree of non-linearity
d_s	1	Degree of freedom for signal
$\boldsymbol{\varepsilon}$	$m \times 1$	Measurement and forward model error
$\boldsymbol{F}$	$m \times 1$	Forward model
$\mathbf{G}$	$n \times m$	Gain matrix
$\mathbf{K}$	$m \times n$	Weighting function matrix
H	1	Information content in bits
λ	1	Wavelength
λ_c	1	Center wavelength of a fit window
$\lambda_{\max}$	1	Maximum wavelength of a fit window
$\lambda_{\min}$	1	Minimum wavelength of a fit window
m	1	Size of measurement vector (=134)
n	1	Size of state vector (=26)
n_b	1	Size of parameter vector
n_{CO_2}	1	CO_2 profile layers (=10)
P	1	Polynomial coefficient
p_s	1	Surface pressure
$\boldsymbol{r}_\sigma$	$n \times 1$	Uncertainty reduction
$\hat{\mathbf{S}}$	$n \times n$	Covariance matrix of retrieved state
$\mathbf{S}_a$	$n \times n$	A priori covariance matrix
$\mathbf{S}_\epsilon$	$m \times m$	Measurement error covariance matrix
$\boldsymbol{w}$	$n \times 1$	Layer weighting vector
$\boldsymbol{x}$	$n \times 1$	State vector
$\boldsymbol{x}_0$	$n \times 1$	First guess state vector
$\boldsymbol{x}_a$	$n \times 1$	a priori state vector
$\boldsymbol{x}_t$	$n \times 1$	True state vector
$\hat{\boldsymbol{x}}$	$n \times 1$	Retrieved state vector
χ^2	1	Cost function (Eq. 2)
$\boldsymbol{y}$	$m \times 1$	Measurement vector

we test for convergence by relating the changes of the state vector to the error covariance $\hat{\mathbf{S}}$ after each iteration. If the value of $(\boldsymbol{x}_i - \boldsymbol{x}_{i+1})^T \hat{\mathbf{S}}^{-1} (\boldsymbol{x}_i - \boldsymbol{x}_{i+1})$ falls below the number of state vector elements (26), we assume that convergence is achieved and stop the iteration. As it is theoretically possible that convergence is never achieved, we stop the iteration after ten unsuccessful steps. However, typically, the convergence criterion is fulfilled after two to four iterations.

Subsequently, we use some terms also given by Rodgers (2000) to compute the gain matrix $\mathbf{G}$ (Eq. 2.45), the averaging kernel matrix $\mathbf{A}$ (Eq. 3.10), the degree of freedom for signal d_s (Eq. 2.80), and the information content H (Eq. 2.80). The gain matrix corresponds to the sensitivity of the retrieval to the measurement and is given by:

$$\mathbf{G} = (\mathbf{K}^T \mathbf{S}_\epsilon^{-1} \mathbf{K} + \mathbf{S}_a^{-1}) \mathbf{K}^T \mathbf{S}_\epsilon^{-1} \tag{5}$$

Having the gain matrix, we can compute the averaging kernel matrix which is the sensitivity of the retrieval to the true state:

$$\mathbf{A} = \mathbf{GK} \tag{6}$$

The degree of freedom for signal corresponds to the number of independent quantities that can be derived from the measurement and is given by:

$$d_s = \mathrm{tr}(\mathbf{A}) \tag{7}$$

The information content gives the number of different atmospheric states that can be distinguished in bits:

$$H = -\frac{1}{2} \ln(|\mathbf{I} - \mathbf{A}|) \tag{8}$$

The degree of freedom as well as the information content can be calculated for arbitrary sub sets of state vector elements by taking only corresponding elements of the averaging kernel matrix into account. Comparing the variances of the retrieved state vector elements with the corresponding a priori variances, the uncertainty reduction $\boldsymbol{r}_\sigma$ of the j^{th} state vector element is defined by:

$$\boldsymbol{r}_{\sigma\, j} = 1 - \sqrt{\hat{\mathbf{S}}_{j,j} / \mathbf{S}_{a\, j,j}} \tag{9}$$

Note: Using merged fit windows instead of performing a CO_2 and a O_2 retrieval independently within two separate fit windows has two main advantages when retrieving state vector elements which have sensitivities in both fit windows. 1) These elements are better constrained because simultaneous fitting implicitly utilizes the knowledge that the retrieved quantity (e.g. the atmospheric temperature) must be identical in both fit windows. 2) If there are state vector elements with strong ambiguities in one fit windows (e.g. surface pressure and scattering parameters in the CO_2 fit window), the information come mainly from the fit window with less ambiguities. Merging the fit windows makes this information available in both fit windows.

3.1 Forward model

All radiative transfer calculations utilized for our studies are calculated with the SCIATRAN 3.0 radiative transfer code (Rozanov et al., 2005) in discrete ordinate mode. We use the correlated-k approach of Buchwitz et al. (2000a) to increase the computational efficiency. As final part of the forward calculation, the resulting spectra are folded with a SCIAMACHY like Gaussian slit function and the dead/bad pixel mask also used for WFM-DOAS 1.0 is applied. Spectral line parameters are taken from the HITRAN 2008 (Rothman et al., 2009) database.

The radiative transfer calculations are performed on 60 model levels, even though our state vector includes only a ten-layered CO_2 mixing ratio profile. This profile is expanded to the model levels before each forward calculation.

In the case of liquid water droplets, phase function, extinction, and scattering coefficient of cloud particles are calculated with Mie's theory assuming gamma particle size distributions.

In the case of ice crystals, corresponding calculations are performed with a Monte Carlo code, assuming an ensemble of randomly aligned fractal or hexagonal particles. The volume scattering function is the product of phase function and scattering coefficient. Figure 3 illustrates the volume scattering functions of all cloud particles analyzed in Sect. 4.

3.2 State vector

All retrieval results shown here are valid for a state vector consisting of 26 elements listed in the first column of Table 3. Corresponding weighting functions calculated for exemplary atmospheric conditions are illustrated in Fig. 4. This figure shows that not only the scattering parameter weighting functions may have cross correlations with other weightung functions. In this context, e.g. the albedo weighting functions show strong similarities to the scattering related weighting functions. For all state vector elements, we aim at obtaining realistic a priori uncertainties which sufficiently constrain the inversion by defining a well-posed problem without dominating the retrieval results.

3.2.1 Wavelength shift, slit function FWHM

The state vector accounts for fitting a wavelength shift and the full width half maximum (FWHM) of a Gaussian shaped instrument's slit function separately in the O_2 and CO_2 fit window. This means, the corresponding weighting functions are identical zero within the O_2 or in the CO_2 fit window, respectively.

3.2.2 Albedo

We assume a Lambertian surface with an albedo α with smooth spectral progression which can be expressed by a 2nd order polynomial separately within both fit windows.

$$\alpha_\lambda = P_0 + P_1 \frac{\lambda - \lambda_c}{\lambda_{\max} - \lambda_{\min}} + P_2 \left(\frac{\lambda - \lambda_c}{\lambda_{\max} - \lambda_{\min}}\right)^2 \qquad (10)$$

Here, P_0, P_1, and P_2 are the polynomial coefficients, λ the wavelength, λ_c the center wavelength, $\lambda_{\min}$ the minimum, and $\lambda_{\max}$ the maximum wavelength within the fit window. In order to get good first guess and a priori estimates for the 0th polynomial coefficients, we use the look-up table based albedo retrieval described by Schneising et al. (2008). This estimates the albedo within a micro window not influenced by gaseous absorption lines at one edge of each fit window assuming a cloud free atmosphere with moderate aerosol load. We use an a priori uncertainty of 0.05 for the 0th polynomial coefficients. The first guess and the a priori values of the 1st and 2nd polynomial coefficients are zero. Their

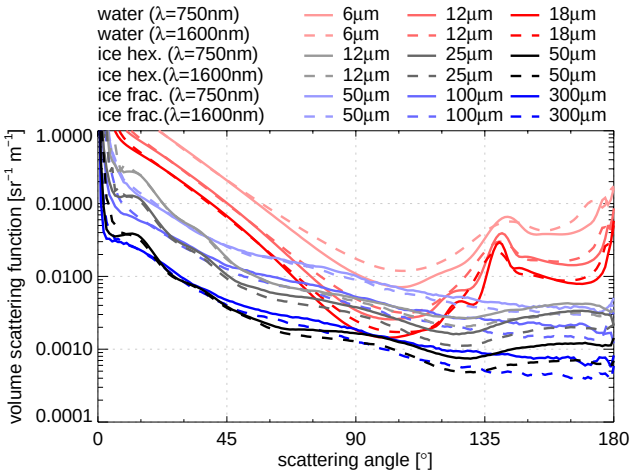

Fig. 3. Volume scattering functions of all cloud particles analyzed in Sect. 4. The dominant forward peaks is cut in this clipping.

estimated a priori uncertainties are 0.01 and 0.001, respectively. The magnitude of these values is typical for 2nd order polynomial coefficients fitted to the natural surfaces albedos shown in Fig. 5.

3.2.3 CO_2 mixing ratio profile

The CO_2 mixing ratio is fitted within 10 atmospheric layers, splitting the atmosphere in equally spaced pressure intervals normalized by the surface pressure p_s $(0.0, 0.1, 0.2, \ldots, 1.0)$.

We analyzed CarbonTracker data over land surfaces of the years 2003 to 2005 to determine a static a priori statistic for the CO_2 mixing ratio in corresponding pressure levels. The resulting a priori state vector elements, their standard deviation and correlation matrix are shown in Fig. 6. It is not surprising that the largest variability is observed in the lowest 10% of the atmosphere. From the correlation matrix it is also visible that there are large cross correlations in the boundary layer, the free troposphere, and the stratosphere.

As the shape of the CO_2 weighting functions in SCIAMACHY resolution shows only minor changes with height, it cannot be expected that there is much information obtainable about the CO_2 profile shape from SCIAMACHY nadir measurements. Therefore, we use a relatively narrow constraint for the profile shape but simultaneously a rather weak constraint for XCO_2. For this reason, we build the CO_2 part of the a priori covariance matrix by using the correlation matrix as is but using a four times increased standard deviation. As a result, the a priori uncertainty of XCO_2 increases from 3.9 to 15.6 ppm. The average XCO_2 of all analyzed CarbonTracker profiles amounts to 376.8 ppm.

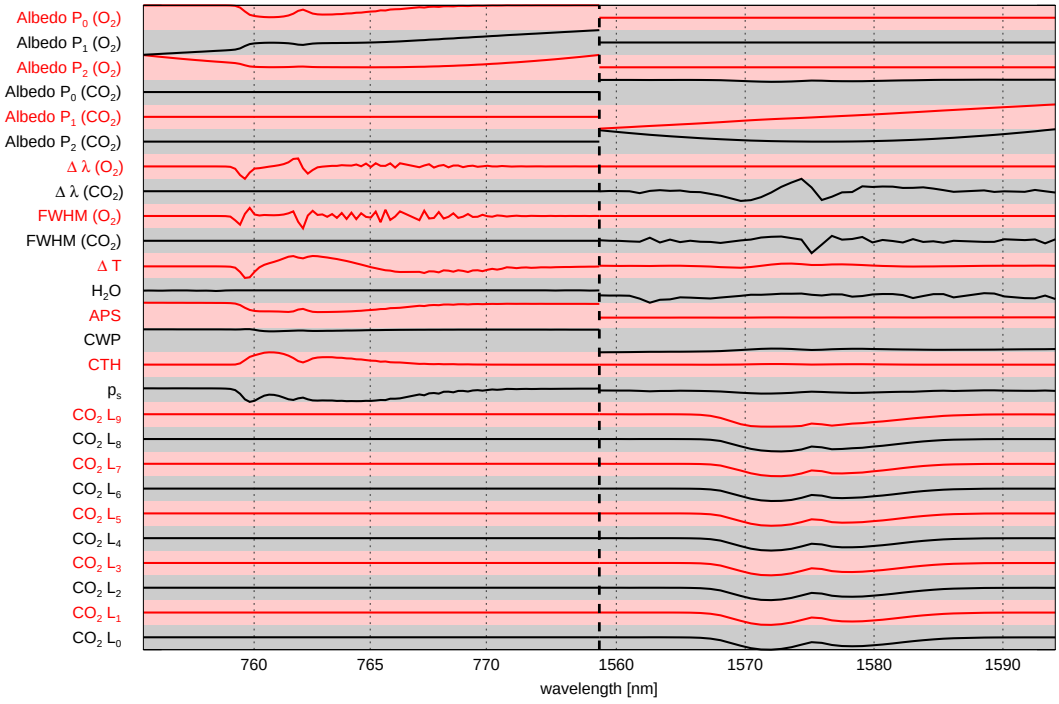

Fig. 4. Weighting functions (scaled to the same amplitude) calculated with the SCIATRAN 3.0 radiative transfer code for the first guess state vector of the "met. 1σ" scenario at 40° solar zenith angle.

3.2.4 Atmospheric profiles

With regard to the application to real SCIAMACHY measurements, we plan to use atmospheric profiles of pressure, temperature, and humidity provided by ECMWF (European Center for Medium-range Weather Forecasts) for the forward model calculations as part of the parameter vector. Applying the hydrostatic assumption, the surface pressure determines the total number of air molecules within the atmospheric column. Therefore, it is a critical parameter for the retrieval of XCO_2.

We compared a dataset of more than 8000 radiosonde measurements of the year 2004 within −70° E to 55° E longitude and −35° N to 80° N latitude with corresponding ECMWF profiles. The exact SCIAMACHY sub pixel composition of surface elevations is not perfectly known. For this reason, we used unmodified ECMWF profiles i.e. we performed no interpolation of the surface height within the ECMWF profiles. Therefore, the surface elevation within a radiosonde profile may differ from the surface elevation within the profile of the corresponding ECMWF grid box. This means, our estimate combines two uncertainties: The ECMWF surface pressure uncertainty and the sub grid box surface pressure variability due to topography which is most times much larger. This is only a rough estimate that certainly drastically overestimates the true ECMWF surface pressure precision for cases where an interpolation to the true topography within the instrument's field of view can be applied. However, this overestimation ensures that we do not over constrain the retrieval in respect to surface pressure.

Resulting from these comparisons, we estimated that the surface pressure is known with a standard deviation of 3.2%. The standard deviation of the temperature shift between measured and modeled temperature profiles amounts to 1.1 K. The corresponding value for a scaling of the H_2O profile is 32%. The biases were much smaller than the standard deviations. Therefore, we apply no bias to the a priori knowledge of surface pressure, temperature profile shift, and scaling of the humidity profile.

3.2.5 Scattering parameters

Scattering can cause very complex modifications of the satellite observed radiance spectra and there is nearly an infinite amount of micro and macro physical parameters that are needed to comprehensively account for all scattering effects in the forward model. However, as illustrated in Figs. 1 and 2 it is unlikely possible to retrieve many of these parameters simultaneously from SCIAMACHY measurements in the O_2 fit window. The same applies to the CO_2 fit window which contains even less information about these parameters.

We concentrate on three macro physical scattering parameters having a dominant influence on the measured spectra. Their weighting functions contain sufficiently unique

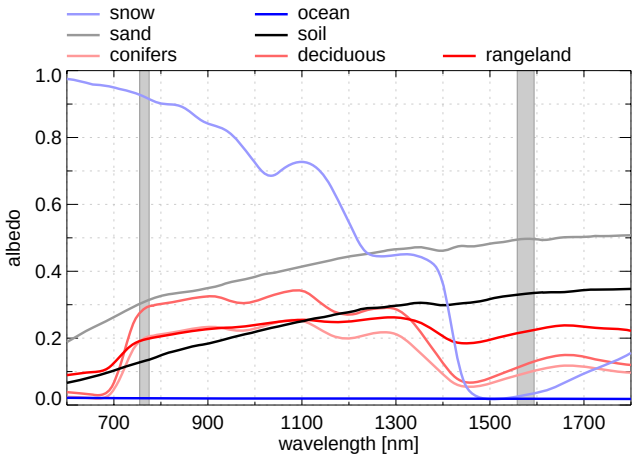

Fig. 5. Spectral albedos of different natural surface types. Reproduced from the ASTER Spectral Library through the courtesy of the Jet Propulsion Laboratory, California Institute of Technology, Pasadena, California (©1999, California Institute of Technology) and the Digital Spectral Library 06 of the US Geological Survey.

spectral signatures which makes them distinguishable from other weighting functions. These parameters are cloud top height, cloud water/ice path whereas water/ice stands for ice and/or liquid water, and the aerosol scaling factor for a default aerosol profile. All other scattering related parameters are not part of the state vector but only part of the parameter vector and are set to constant values.

Within the parameter vector we define that scattering at particles takes place in a plane parallel geometry at one cloud layer with a geometrical thickness of 0.5 km homogeneously consisting of fractal ice crystals with 50 µm effective radius. In addition, scattering happens at a standard LOWTRAN summer aerosol profile with moderate rural aerosol load and Henyey-Greenstein phase function and a total aerosol optical thickness of about 0.136 at 750 nm and 0.038 at 1550 nm. Both cloud parameters are aimed at optically thin cirrus clouds because on the one hand it is not possible to get enough information from below an optically thick cloud and on the other hand the foregoing cloud screening filters already the optically thick clouds. Additionally, Schneising et al. (2008) found that thin cirrus clouds are most likely the reason for shortcoming of the WFM-DOAS 1.0 CO_2 retrieval on the Southern Hemisphere.

We set the a priori value of CTH to 10 km with a one sigma uncertainty of 5 km. Both values are only rough estimates for typical thin cirrus clouds. Nevertheless, the size of the one sigma uncertainty seems to be large enough to avoid overconstraining the problem as it covers large parts of the upper troposphere where these clouds occur.

All micro physical cloud and aerosol parameters are assumed to be constant and known. This assumption is obviously not true. Scattering strongly depends on the size of the scattering particles e.g. scattering is more effective at clouds

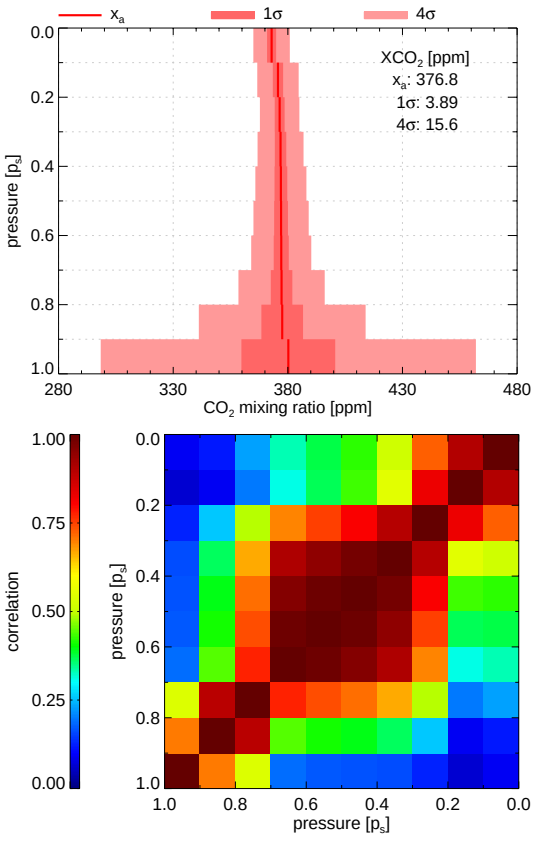

Fig. 6. Static a priori knowledge of the ten-layered CO_2 mixing ratio profile calculated from three years (2003–2005) CarbonTracker data over land surfaces. Top: A priori state vector values and their 1σ and 4σ uncertainties. Bottom: Correlation matrix.

with smaller particles. For this reason, it is not possible to derive the correct cloud water/ice path without knowing the true phase function, scattering, and extinction coefficient of the scattering particles. Hence, the cloud water/ice path parameter, which is part of our state vector, is rather an effective cloud water/ice path corresponding to the particles defined in the parameter vector. As an example, it can be expected that the retrieved CWP will be larger than the true CWP in cases with true particles that are smaller than the assumed particles. Such effects must be considered when choosing the a priori constraints of CWP. Additionally, the constraints must be weak enough to enable cloud free cases with CWP=0. We here use an a priori value for CWP of 5 g/m^2 with an one sigma uncertainty of 10 g/m^2. This corresponds to a cloud optical thicknesses of the a priori cloud of 0.16. For the aerosol scaling factor we use an a priori value of 1.0 with a standard deviation of 1.0.

Obviously, three parameters are by far not sufficient to describe all forms of scattering that can influence the SCIAMACHY measurements. However, we are not aiming to retrieve a very accurate and complete set of cloud or aerosol parameters. Therefore, we will address as major topic of

Sect. 4 the question how the lack of knowledge about several macro and micro physical cloud properties affects the XCO_2 results.

3.3 XCO_2

In this section we describe how XCO_2 is calculated from the retrieved state vector elements and what implications this calculations have for the error propagation. As mentioned before, the CO_2 mixing ratio profile consists of ten layers with equally spaced pressure levels at $(0.0, 0.1, 0.2, \ldots, 1.0)\, p_s$. Under the assumption of hydrostatic equilibrium, each layer consists of the same number of air molecules. We define the layer weighting vector $\boldsymbol{w}$ as the fraction of air molecules in each layer compared to the whole column. In our case its value is always 0.1. For all elements that do not correspond to a CO_2 mixing ratio profile element in the state vector, the layer weighting vector is zero. XCO_2 is than simply calculated by:

$$XCO_2 = \boldsymbol{w}^T \hat{\boldsymbol{x}} \tag{11}$$

Following the rules of error propagation, the variance of the retrieved XCO_2 is given by:

$$\sigma^2_{XCO_2} = \boldsymbol{w}^T \hat{\mathbf{S}} \boldsymbol{w} \tag{12}$$

Note: the surface pressure weighting function is defined in that way, that a modification of the surface pressure influences the number of molecules in the lowest layer only. This means, after an iteration that modifies the surface pressure, the surface layer will not have the same number of air molecules anymore. The surface pressure weighting function expands or reduces the lowest layer assuming that this layer has a CO_2 mixing ratio given by the latter iteration or the first guess value. Therefore, the surface pressure weighting function influences the mixing ratio which is now a weighted average of the mixing ratio before and after iteration. For this reason, at the end of each iteration, the new non-equidistant CO_2 mixing ratio profile, which now starts at the updated surface pressure, is interpolated to ten equidistant pressure levels whereas XCO_2 is conserved.

4 Error analysis

Within the error analysis, the retrieval algorithm is applied to SCIAMACHY measurements simulated with the forward model described in Sect. 3.1 using a modified US-standard atmosphere. The corresponding measurement error covariance matrices are assumed to be diagonal. They are calculated for an exposure time of 0.25 s using the instrument simulator that was also used for the calculations of Buchwitz and Burrows (2004). However, it shall be noted that the calculated measurement errors are not utilized for adding noise to the simulated spectra.

In the following, we analyze the retrieval's capability to reproduce the state vector elements as well as the retrieval's sensitivity to cloud and aerosol related parameter vector elements. Therefore, we define a set of 35 test scenarios. Some of them are only aiming at the retrieval's capability to reproduce changes of state vector elements.

However, radiative transfer through a scattering atmosphere can be very complex. Thinking about the almost infinite number of possible ensembles of scattering particles, all with different phase functions, extinction, and absorption coefficients, a set of three scattering related state vector elements is by far not enough to comprehensively describe all possible scattering effects. For this reason, the remaining test scenarios are used to estimate the sensitivity to aerosol, cloud micro and macro physical parameters which are not part of the state vector but of the parameter vector.

An overview of the results of all test scenarios is given in Table 2 showing the systematic and stochastic XCO_2 errors of all scenarios for the solar zenith angles (SZA) 20°, 40°, and 60°. Additionally, the systematic and stochastic errors of the scattering parameters and the surface pressure are given for 40° SZA. Except for the "spectral albedo" scenarios, all calculations are performed with an spectrally constant Lambertian albedo of 0.2. Table A1 and Table A2 include corresponding results but for calculations with an albedo of 0.1 and 0.3, respectively.

Note: The stochastic errors represent the a posteriori errors based on the assumed measurement noise and the assumed a priori error covariance matrix. According to Eq. (3.16) of Rodgers (2000), the systematic errors given in Table 2 correspond to the smoothing error $(\mathbf{A}-\mathbf{I})(\boldsymbol{x}_t - \boldsymbol{x}_a)$ of the state vector elements. This applies to all scenarios in which only state vector elements but no parameter vector elements are modified. In these cases, errors due to noise, unknown parameter vector elements, and due to the forward model do not exist.

4.1 The "dry run" scenario

The true state vector of the "dry run" scenario is almost identical to the first guess state vector which is again identical to the a priori state vector in almost all elements. Only the constant part of the albedo polynomials of the first guess state vector differ slightly from the true state vector as it is estimated by the prior first guess albedo retrieval mentioned in Sect. 3.2.2. The "dry run" scenario includes a thin cirrus cloud with a CTH of 10 km, a CWP of 10 g/m^2, and a COT at 500 nm of 0.33.

Residuals with relative root mean square (RMS) values below 0.005‰ in the O_2 and CO_2 region as well as almost no systematic errors prove that the algorithm is self-consistent (Table 2).

The "dry run" scenario serves as basis for several other scenarios which are mainly intended to quantify the retrievals capability of reproducing modifications to a specific state vector element or to quantify the retrievals sensitivity to a specific parameter vector element.

Table 2. Overview of the retrieval performance for 35 test scenarios based on SCIATRAN 3.0 simulations with a modified US-standard atmosphere. For all scenarios, we assume a Lambertian surface with an albedo which is spectrally constant 0.2 except for the "spectral albedo" scenarios. The table shows the average signal to noise (SNR) and the residuals relative root mean square (RMS) in both fit windows as well as the main retrieval errors of XCO_2, scattering parameters (CWP, CTH, APS), and surface pressure. All errors are given with systematic error (bias) ±stochastic error. The scenarios are based on the "dry run" scenario (♣), the "met. 1σ" scenario (♦), and the "no cloud" scenario (♥). Some scenarios are intended to quantify the retrievals capability of reproducing modifications of state vector elements (❍). The other scenarios are intended to additionally quantify the retrievals sensitivity to parameter vector elements (❑) (i.e. to a imperfect forward model).

Scenario	SNR		RMS [‰]		SZA 40°					SZA 20°	SZA 60°
	O_2	CO_2	O_2	CO_2	p_s [hPa]	CWP [g/m^2]	CTH [km]	APS	XCO_2 [ppm]	XCO_2 [ppm]	XCO_2 [ppm]
dry run ❍	1560	1116	0.00	0.00	0±7	−0.1±1.1	0.0±0.4	0.0±0.7	0.1±3.2	0.1±3.1	0.0±3.3
met. 1σ ❍	1645	1078	0.04	0.06	4±6	0.6±0.7	−0.3±0.4	−0.6±0.7	−2.4±3.4	−3.2±3.4	−1.2±4.0
calibration ♣,❑	1659	1190	0.04	0.01	−5±6	0.9±1.0	0.2±0.4	−0.1±0.6	0.8±3.1	0.8±3.1	0.9±3.1
CO_2 profile											
plus 1σ ♣,❍	1560	1114	0.03	0.05	0±7	0.1±1.1	−0.0±0.4	−0.0±0.7	−1.5±3.5	−1.4±3.5	−1.6±3.5
plus 3σ ♣,❍	1560	1110	0.08	0.14	5±7	0.8±1.1	−0.2±0.4	−0.4±0.6	−5.7±4.4	−5.6±4.4	−5.1±3.9
art. profile ♣,❍	1560	1115	0.03	0.04	0±7	−0.0±1.1	0.0±0.4	0.0±0.7	−1.2±3.4	−1.1±3.4	−1.3±3.4
Spectral albedo											
sand ♣,❍	1966	1950	0.02	0.05	0±5	−0.2±1.0	0.1±0.4	0.1±0.7	−0.2±3.0	−0.1±3.0	−0.5±2.6
soil ♣,❍	1264	1531	0.01	0.01	0±8	−0.1±1.0	0.0±0.4	0.0±0.6	0.1±3.9	0.2±3.9	−0.2±3.5
deciduous ♣,❍	1891	808	0.02	0.01	−1±5	−0.2±1.0	0.1±0.4	0.1±0.7	−0.2±3.5	−0.1±3.3	−0.8±4.8
conifers ♣,❍	1557	694	0.02	0.01	−1±7	−0.2±1.1	0.1±0.4	0.1±0.7	−0.2±4.1	−0.1±3.7	−0.5±5.6
rangeland ♣,❍	1542	1182	0.01	0.00	0±7	−0.1±1.1	0.0±0.4	0.0±0.7	0.1±3.2	0.2±3.2	0.1±3.2
snow ♣,❍	3622	348	0.00	0.18	0±3	−0.0±0.4	0.0±0.3	0.0±0.3	0.5±7.9	−0.7±7.1	−0.3±10.4
ocean ♣,❍	640	279	0.01	0.00	0±21	−0.0±0.7	0.0±0.3	0.0±0.5	0.0±10.3	0.0±9.4	0.6±12.3
Macro physical cloud properties											
no cloud ♣,❍	1492	1195	0.03	0.01	−1±4	0.0±0.8	10.0±5.0	−0.0±0.6	−0.4±3.3	−0.5±3.6	−0.4±3.0
CWP 0.3 ♣,❍	1493	1193	0.03	0.01	0±4	0.1±0.9	−0.0±4.7	−0.0±0.7	−0.5±3.3	−0.5±3.5	−0.4±3.1
CWP 3.0 ♣,❍	1508	1170	0.02	0.00	0±6	0.0±1.3	0.0±1.5	0.0±0.7	−0.2±3.4	−0.2±3.4	−0.2±3.1
CWP 30.0 ♣,❍	1756	997	0.03	0.02	−5±6	−0.3±0.7	0.0±0.1	0.2±0.7	−0.3±3.4	0.3±3.2	0.0±4.2
CTH 3 ♣,❍	1543	1116	0.17	0.02	0±5	−8.0±1.9	2.2±2.9	−0.0±0.9	−0.5±3.7	−1.0±3.7	0.3±3.3
CTH 6 ♣,❍	1550	1116	0.05	0.00	−2±6	−0.6±2.1	0.1±0.7	0.0±0.8	0.3±3.3	0.2±3.3	0.4±3.5
CTH 12 ♣,❍	1564	1116	0.01	0.00	0±6	−0.0±0.8	−0.0±0.5	0.0±0.7	0.1±3.1	0.1±3.1	−0.2±3.3
CTH 21 ♣,❍	1575	1116	0.07	0.00	0±3	0.1±0.3	−0.6±1.1	−0.0±0.4	−0.1±2.9	−0.1±2.8	−0.1±3.4
CFC 50 ♦,❑	1577	1134	0.09	0.04	0±6	−5.8±0.8	−0.6±0.8	−1.2±0.6	−5.1±3.5	−6.0±3.5	−0.3±3.4
CGT ♦,❑	1641	1078	0.05	0.06	3±6	0.6±0.7	−1.6±0.3	−0.6±0.7	−2.9±3.3	−3.3±3.4	−1.6±4.0
multilayer ♦,❑	1626	1078	0.13	0.06	0±5	−1.4±1.0	0.2±0.3	−0.3±0.8	−2.1±3.3	−2.8±3.3	−1.6±4.2
Micro physical cloud properties											
ice frac. 100 ♦,❑	1575	1126	0.06	0.05	5±6	−5.8±0.8	−0.8±0.7	−0.9±0.7	−1.5±3.4	−3.4±3.4	6.1±3.6
ice frac. 300 ♦,❑	1528	1166	0.08	0.05	6±6	−10.9±1.0	−2.1±1.3	−1.0±0.7	−3.2±3.6	−4.3±3.6	2.2±3.3
ice hex. 25 ♦,❑	1614	1137	0.06	0.06	5±6	5.0±0.7	−0.3±0.5	−0.7±0.7	−0.3±3.4	−3.2±3.5	3.9±3.7
ice hex. 50 ♦,❑	1575	1122	0.06	0.07	3±6	1.5±0.8	−0.7±0.7	−1.0±0.7	0.8±3.5	−0.9±3.6	8.3±3.6
water 6 ♦,❑	1613	1281	0.18	0.06	−1±6	−0.6±1.6	5.9±1.9	−1.2±0.8	−5.3±4.0	−7.6±3.8	−5.0±3.3
water 12 ♦,❑	1559	1236	0.28	0.05	1±5	−1.1±1.7	5.1±2.4	−1.0±0.8	−4.5±4.1	−3.4±4.0	−0.5±3.4
water 18 ♦,❑	1541	1220	0.12	0.05	2±5	−0.9±1.6	5.1±2.3	−1.1±0.8	−5.4±4.0	−3.5±4.0	−0.3±3.4
Aerosol											
OPAC background ♥,❑	1492	1197	0.02	0.01	−1±4	0.0±0.7	10.0±5.0	−0.2±0.6	−0.3±3.3	−0.1±3.6	−0.6±3.0
OPAC urban ♥,❑	1452	1177	0.08	0.01	0±4	0.1±0.6	10.1±5.0	−0.3±0.6	−0.3±3.2	−0.2±3.5	−0.0±3.1
OPAC desert ♥,❑	1491	1200	0.04	0.00	2±4	−0.1±0.8	10.0±5.0	0.1±0.7	0.2±3.4	0.2±3.7	0.3±3.0
extreme in BL ♥,❑	1609	1139	0.16	0.05	−11±5	0.6±1.5	7.1±4.0	0.3±0.8	6.5±3.8	2.9±3.8	13.9±3.4

4.2 The "met. 1σ" scenario

The meteorological parameters (temperature shift, H_2O scaling, APS, CWP, CTH, p_s, and CO_2 mixing ratio) of the true state vector of the "met. 1σ" scenario differ from the corresponding values of the a priori state vector by 0.5 to 1.0 sigma a priori uncertainty. The "met. 1σ" scenario includes a thin cirrus cloud with a CTH of 15 km, a CWP of 15 g/m^2, and a COT at 500 nm of 0.49.

In detail, the true, a priori, and first guess state vector as well as the retrieved state vector and corresponding values of degree of freedom, information content, and uncertainty

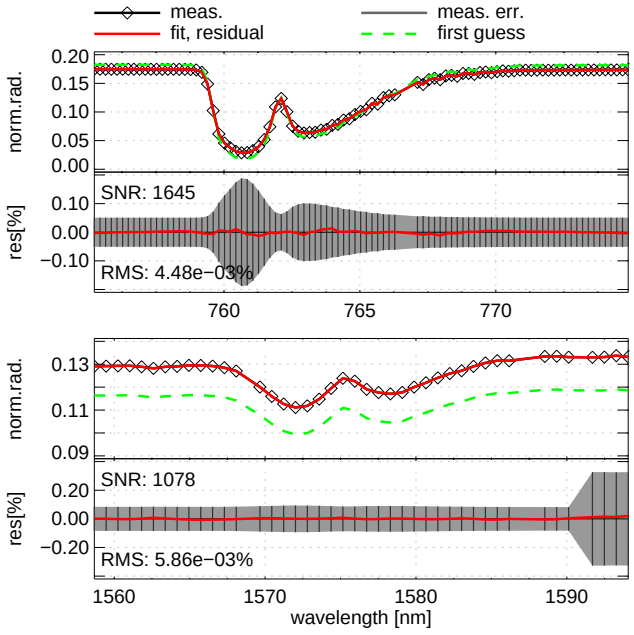

Fig. 7. O_2 and CO_2 fit windows with simulated measurements, first guess, fitted sun-normalized radiation, residual and simulated measurement uncertainty for the "met. 1σ" scenario at 40° solar zenith angle.

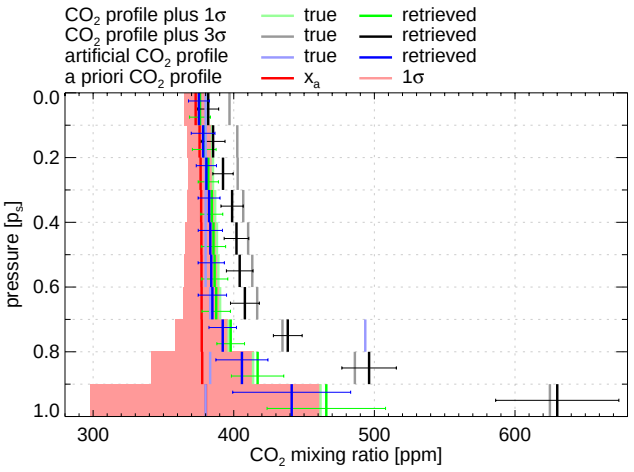

Fig. 8. Retrieved and true CO_2 mixing ratio profiles of the three "CO_2 profile" scenarios.

reduction are given for this scenario in Table 3. The corresponding spectral fits in both fit windows as well as their residuals are plotted in Fig. 7.

We find large uncertainty reductions greater than 0.88 for the albedo parameters, wavelength shift, and FWHM within the O_2 spectral region. The corresponding values of the CO_2 spectral region are somewhat smaller but always greater equal 0.69. Temperature shift and H_2O scaling are retrieved with low systematic biases and error reductions of 0.67 and 0.79 despite rather narrow a priori constraints.

In contrast to this, the APS retrieval, with an uncertainty reduction of only 0.32, seems to be dominated by the a priori even though the corresponding constraints are weak. Accordingly, we find a large stochastic error of 0.7 and a large systematic bias of -0.6 which brings the retrieval close to the a priori value. This can be explained by the following: The aerosol profile has its maximum in the boundary layer and scattering and absorption features of aerosol vary only slowly in the relatively narrow fit windows. Therefore, it is not surprising that the shape of the APS weighting function has similarities to the surface pressure weighting function. Additionally, the sensitivity to APS is very low due to very low absolute values of the APS weighting function. For both points see Fig. 2.

Compared to APS, the error reduction of CWP and CTH is much higher (>0.9). Referring to Fig. 2, the shape of the CWP weighting function strongly depends on the specific scenario which can cause ambiguities, problems of finding suitable first guess values, and problems of the convergence behavior. The retrieval's sensitivity to CWP and CTH is described in more detail in Sect. 4.6.

The surface pressure is retrieved with a bias of 4 hPa, a stochastic error of 6 hPa and an error reduction of 0.80. As the CO_2 layered weighting functions look very similar and as the a priori knowledge shows strong inter-correlation between the layers, the retrieved profile has also strongly correlated layers. Additionally, the retrieval shows a very low error reduction especially in the stratosphere resulting in a degree of freedom for signal of 1.07 for the whole profile. This means that only one independent information can be retrieved about the profile. The shape of the profile remains strongly dominated by the a priori statistics. See also Sects. 4.4 and 4.9.

The "met. 1σ" scenario serves as basis for several other scenarios which are mainly intended to quantify the retrievals performance under more realistic conditions including also unknown parameter vector elements, i.e. an imperfect forward model.

4.3 Calibration

The state vector of the WFM-DOAS algorithm includes a polynomial which accounts, among others, for spectrally smooth variations of the surface albedo and for calibration errors causing a scaling of the sun-normalized radiance. Solely the albedo retrieval of the WFM-DOAS algorithm relies on an absolute calibration. However, the WFM-DOAS albedo retrieval will produce unrealistic results in the presence of clouds. For this reason, our method follows a slightly different approach by fitting the albedo with a 2nd order polynomial. The "calibration" scenario estimates the influence of calibration errors that cause an intensity scaling. For this purpose, the simulated intensity of the "dry run" was scaled

Table 3. Detailed retrieval results of the "met. 1σ" scenario for each state vector element and for the resulting XCO_2. The meaning of the columns from left to right is: 1) name of the state vector element, 2+3) weighting function with non-zero elements in the O_2 and CO_2 fit window, respectively, 4) true state $\boldsymbol{x}_t$, 5) first guess state $\boldsymbol{x}_0$, 6) a priori state $\boldsymbol{x}_a$ ±uncertainty, 7) retrieved state $\hat{\boldsymbol{x}}$ ±stochastic error, 8) information content H, 9) degree of freedom for signal d_s, 10) uncertainty reduction $\boldsymbol{r}_\sigma$ Note: $\boldsymbol{x}_t$, $\boldsymbol{x}_0$, $\boldsymbol{x}_a$, $\hat{\boldsymbol{x}}$, and the corresponding errors are rounded to the same number of digits within each line.

Name	O_2	CO_2	$\boldsymbol{x}_t$	$\boldsymbol{x}_0$	$\boldsymbol{x}_a$	$\hat{\boldsymbol{x}}$	H [bit]	d_s	$\boldsymbol{r}_\sigma$
Albedo P_0	•		0.200	0.224	0.224 ± 0.050	0.202 ± 0.002	4.65	1.00	0.96
Albedo P_1	•		0.0000	0.0000	0.0000 ± 0.0100	0.0000 ± 0.0001	6.73	1.00	0.99
Albedo P_2	•		0.0000	0.0000	0.0000 ± 0.0010	0.0000 ± 0.0001	3.09	0.99	0.88
Albedo P_0		•	0.200	0.168	0.168 ± 0.050	0.201 ± 0.001	5.62	1.00	0.98
Albedo P_1		•	0.0000	0.0000	0.0000 ± 0.0100	0.0000 ± 0.0002	5.63	1.00	0.98
Albedo P_2		•	0.0000	0.0000	0.0000 ± 0.0010	0.0001 ± 0.0003	1.92	0.93	0.74
$\Delta\lambda$ [nm]	•		0.000	0.000	0.000 ± 0.100	0.000 ± 0.000	9.14	1.00	1.00
$\Delta\lambda$ [nm]		•	0.000	0.000	0.000 ± 0.100	0.001 ± 0.007	3.77	0.99	0.93
FWHM [nm]	•		0.450	0.450	0.450 ± 0.050	0.450 ± 0.000	6.76	1.00	0.99
FWHM [nm]		•	1.400	1.400	1.400 ± 0.100	1.397 ± 0.031	1.68	0.90	0.69
ΔT [K]	•	•	−0.6	0.0	0.0 ± 1.1	-0.8 ± 0.4	1.62	0.89	0.67
H_2O [‰]	•	•	2.70	2.22	2.22 ± 0.86	2.65 ± 0.18	2.26	0.96	0.79
APS	•	•	2.0	1.0	1.0 ± 1.0	1.4 ± 0.7	0.56	0.54	0.32
CWP [g/m^2]	•	•	15.0	10.0	5.0 ± 10.0	15.6 ± 0.7	3.85	1.00	0.93
CTH [km]	•	•	15.0	10.0	10.0 ± 5.0	14.7 ± 0.4	3.59	0.99	0.92
p_s [hPa]	•	•	981	1013	1013 ± 30	985 ± 6	2.33	0.96	0.80
CO_2 L_9 [ppm]		•	380.9	373.0	372.9 ± 8.0	375.4 ± 7.5	0.01	0.01	0.06
CO_2 L_8 [ppm]		•	384.5	375.6	375.7 ± 9.0	378.3 ± 8.5	0.02	0.02	0.06
CO_2 L_7 [ppm]		•	385.1	376.4	376.4 ± 8.6	380.9 ± 7.3	0.03	0.04	0.16
CO_2 L_6 [ppm]		•	386.6	376.8	376.8 ± 10.0	383.0 ± 7.9	0.03	0.04	0.21
CO_2 L_5 [ppm]		•	387.9	377.0	377.0 ± 11.1	384.0 ± 8.7	0.03	0.05	0.22
CO_2 L_4 [ppm]		•	388.9	377.0	377.0 ± 12.0	384.7 ± 9.4	0.04	0.05	0.22
CO_2 L_3 [ppm]		•	390.0	377.1	377.1 ± 13.1	385.7 ± 10.2	0.04	0.05	0.22
CO_2 L_2 [ppm]		•	394.7	377.3	377.3 ± 18.8	394.7 ± 9.8	0.08	0.10	0.48
CO_2 L_1 [ppm]		•	409.3	377.6	377.6 ± 36.4	411.5 ± 18.5	0.17	0.21	0.49
CO_2 L_0 [ppm]		•	448.0	380.2	380.2 ± 81.8	453.6 ± 42.0	0.50	0.50	0.49
XCO_2 [ppm]			395.6	376.8	376.8 ± 15.6	393.2 ± 3.4	2.46	1.07	0.78

by a factor by 10%. This primarily affects the retrieved 0th order albedo polynomials which are approximately 10% too large. The weighting function of the 0th order albedo polynomial shows similarities with other weighting functions (Fig. 4) which affects the retrieval errors of other parameters. However, the systematic errors of XCO_2 remain smaller than 1 ppm.

4.4 CO_2 profile

The detailed results of the "met. 1σ" scenario, given in Table 3, already show that it is not possible to retrieve much information about the profile shape. Figure 8 shows the retrieved CO_2 profiles of the "plus 1σ", "plus 3σ", and "art. profile" CO_2 profile scenarios. The three scenarios differ from the "dry run" scenario only by a modified (true) CO_2 profile.

The "plus 1σ" scenario has a true CO_2 profile which differs from the a priori profile by an enhancement of 1σ a priori uncertainty in each layer. We find a slight overestimation of the CO_2 mixing ratio in the boundary layer, an almost neutral behavior between $0.8\,p_s$ and $0.3\,p_s$, and a slight underestimation in the stratosphere. The resulting XCO_2 has a bias of -1.5 ppm and a stochastic error of 3.5 ppm for 40° SZA (Table 2).

In the case of the "plus 3σ" scenario, the observed effects become more pronounced. We find a week overestimation in the boundary layer, a week underestimation between $0.8\,p_s$ and $0.3\,p_s$, and a clear underestimation in the stratosphere. The resulting XCO_2 has a bias of -5.7 ppm and a stochastic error of 4.4 ppm (Table 2). Even though this scenario is a clear outlier in terms of the a priori statistics, the algorithm is still able to retrieve XCO_2 with a systematic absolute error of 1.5%. This means that the XCO_2 retrieval is still dominated by the measurement but not by the a priori constraint. However, low uncertainty reductions in the stratospheric layers as well as the fact that the retrieved mixing ratios are much closer to the a priori than to the true profile show that the stratospheric layers are dominated by the a priori information and not by the measurement.

In order to illustrate that it is actually not possible to retrieve the shape of the CO_2 profile, we confront the retrieval with an artificial profile with an almost constant mixing ratio of 380 ppm in all layers except the third layer having a mixing ratio of about 495 ppm. In this case, the retrieved CO_2 profile follows not the true profile. In fact, the retrieved profile still adopts the shape from the a priori information even though the direction of the profile modification is retrieved correctly. However, the a priori information of the CO_2 profile, which we generate from CarbonTracker data, hint that the profile shape is already relatively well known before the measurement (Fig. 6). Therefore, it is most unlikely that scenarios like the "art. profile" scenario occur in reality.

Note that the systematic errors shown in this subsection correspond to the CO_2 profile smoothing error.

4.5 Spectral albedo

Unfortunately, the spectral albedo cannot be assumed to be constant within the O_2 and CO_2 fit window. In the worst case, the spectral shape of the albedo would be highly correlated with the surface pressure or CO_2 weighting function. In this case, errors of the retrieved surface pressure or CO_2 mixing ratios would be unavoidable. However, this is most unlikely in reality.

As illustrated in Fig. 5, the albedo of typical surface types is spectrally smooth and only slowly varying within the fit windows. This applies especially to satellite pixels with large foot print size consisting of a mixture of surface types. Therefore, we assume that the albedo can be approximated within each fit window with a 2nd order polynomial. In order to make a perfect retrieval with no remaining residuals theoretically possible, we fit a 2nd order polynomial in both fit windows to the spectral albedos given in Fig. 5. We use these polynomials as true spectral albedo for the albedo scenarios "sand", "soil", "deciduous", "conifers", "rangeland", "snow", and "ocean". All other elements of the state vector are identical to those of the "dry run" scenario.

Table 2 shows that the systematic XCO_2 errors of these scenarios are all between -0.8 and 0.6 ppm, most of them close to zero. We observe almost no systematic errors for the surface pressure. According to the large differences of the tested albedos, SNR values vary from 640 to 3622 in the O_2 fit window and from 279 to 1950 in the CO_2 fit window.

We find the lowest stochastic XCO_2 errors for the "sand" scenario. This scenario has a relatively high albedo of about 0.3 in the O_2 and 0.5 in the CO_2 fit window. For this reason the corresponding SNR values are also relatively large which is essential for low stochastic errors.

The largest SNR values are observed in the O_2 fit window for the "snow" scenario because of the high reflectivity of snow in this spectral region. Due to the higher spectral resolution, stronger absorption features, and most times better SNR values in the O_2 fit window, the surface pressure retrieval is dominated by the O_2 fit window. For this reason, we observe a distinctively smaller stochastic surface pressure error of 3 hPa for this scenario. Nevertheless, the stochastic XCO_2 error of this scenario is quite large with about 8 ppm. This can be explained by a very low SNR value in the CO_2 fit window caused by a very low reflectivity of snow in this spectral region.

The "ocean" scenario has the lowest albedo and therefore the lowest SNR value in the O_2 and CO_2 fit window. Consequently, we here observe the largest stochastic errors of 21 hPa for the surface pressure and of about 10 ppm for XCO_2. Comparing these values with the uncertainty of the prior knowledge shows that only very little information about XCO_2 can be obtained over snow covered or ocean surfaces.

4.6 Macro physical cloud parameter

Within the scenarios "no cloud", "CWP 0.3" to "CWP 30.0", we test the retrievals ability to retrieve CWP of an ice cloud of fractal particles with 50 µm effective radius (as defined in the parameter vector). All other state vector elements are defined as in the "dry run" scenario. As implied by the name of these scenarios, the ice content of the analyzed clouds amounts to 0.0, 0.3, 3.0, and 30.0 g/m^2. The corresponding cloud optical thicknesses of these scenarios are about 0.00, 0.01, 0.10, and 1.00. Note, in this context, specifying only the optical thickness is not appropriate to describe the scattering behavior of a cloud. Knowledge about phase function, extinction, and absorption coefficients is required in order to make the optical thickness a meaningful quantity. The SNR values of the "no cloud" and "CWP 0.3" scenarios is almost identical and there are only weak differences to the "CWP 3.0" scenario. This indicates that the clouds of these cases are extremely transparent and most likely not visible for the human eye. In contrast to this, the SNR of the "CWP 30.0" scenario increases within the O_2 fit window. Within the CO_2 fit window, the effect of enhanced backscattered radiation is balanced by the strong absorption of ice in this spectral region. We observe nearly no systematic errors of the retrieved surface pressure except for the "CWP 30.0" scenario which results in a bias of -5 hPa. The CWP retrieval is almost bias free compared to its stochastic error for all analyzed solar zenith angles. The same applies to the retrieved CTH of the "CWP" scenarios. For the "no cloud" scenario, the unmodified a priori value is retrieved without any error reduction which is reasonable. The stochastic CTH error reduces for CWP values greater than 3.0 g/m^2. The systematic absolute XCO_2 error of these scenarios is less or equal 0.5 ppm whereas the stochastic error is in the range of 3.0 and 4.2 ppm. In contrast to this, a WFM-DOAS like retrieval systematically overestimates XCO_2 by 3, 33, and more than 400 ppm for the "CWP 0.3", "CWP 3.0", and "CWP 30.0" scenario, respectively. However, the WFM-DOAS 1.0 processing chain filters out cloud contaminated scenarios like the latter. Note, the algorithm gets more and more convergence problems for CWP values larger than

30.0 g/m^2 especially for large solar zenith angles. In such cases, the algorithm is often not able to discriminate between a thick cloud or an extremely low surface pressure.

Analogous to the "CWP" scenarios, the "CTH" scenarios are identical to the "dry run" scenario except for the cloud top height which varies between 3, 6, 12, and 21 km. CWP, CTH, and APS are retrieved nearly bias free for the "CTH 6", "CTH 12", and "CTH 21" scenario. The systematic XCO_2 error of these scenarios is also comparatively low with values between -0.2 and 0.4 ppm. Only the "CTH 3" scenario produces larger systematic errors of CWP and CTH. Additionally, the systematic XCO_2 error of this scenario is slightly larger with values up to -1.0 ppm. This behavior may be explained by the fact that APS, and especially CTH and CWP weighing functions become more and more similar for low clouds.

Up to this point, we only tested the retrieval's ability to reproduce modifications to state vector elements. However, and as mentioned before, especially in respect to scattering, three state vector elements are by far not enough to entirely define the radiative transfer. For this reason, we analyze the retrieval's sensitivity to different parameter vector elements within the following scenarios. At this, we put the emphasis on properties of thin cirrus clouds. In the context of macro physical cloud parameters we estimate the retrieval's sensitivity to cloud fractional coverage of 50% ("CFC 50" scenario), cloud geometrical thickness ("CGT" scenario), and multilayer clouds ("multilayer" scenario). These three scenarios are based on the "met. 1σ" scenario. They only differ from their reference scenario by modified cloud properties.

The radiation of the "CFC 50" scenario is an average of the radiation of the "met. 1σ" scenario with and without cloud. We observe a systematic CWP error being 6.4 g/m^2 smaller than the corresponding error of the "met. 1σ" reference scenario. This can be explained with the total ice content of the "CFC 50" scenario which is 7.5 but not 15 g/m^2. We retrieve XCO_2 values systematically differing in the range of -2.8 and 0.9 ppm from those of the reference scenario. This implies that the errors induced by fractional cloud coverage may also depend on CWP because the modeled cloud appears thicker or thinner under different solar zenith angles. The total XCO_2 errors are here in the range of -6.0 and -0.3 ppm.

The "CGT" scenario differs from the reference scenario only by the cloud geometrical thickness that is 2.5 km compared to 0.5 km for the reference scenario. The results of this scenario are very similar to the reference results. Solely, the retrieved CTH is systematically 1.3 km lower. Due to the larger geometrical thickness and identical ice content at the same time, the particle density is lower. For this reason, the effective penetration depth in this cloud is larger which can explain the differences of the retrieved CTH.

The "multilayer" scenario includes two clouds with identical ice particles and identical geometrical thickness of 0.5 km. The lower CTH is 8 km whereas the upper CTH is 12 km. The corresponding "true" value, which is the basis for the calculation of the CTH bias in Table 2, amounts to 10 km. The results of this scenario are also comparable with the results of the reference scenario. Systematic XCO_2 differences compared to the reference scenario are in the range of -0.4 and 0.4 ppm. The retrieved CTH lies between the simulated clouds and is 0.2 km larger than the average CTH of both cloud layers.

4.7 Micro physical cloud parameter

Within this section we estimate the retrieval's sensitivity to cloud micro physical properties. This means, we confront the retrieval with clouds consisting of particles differing from those defined in the parameter vector.

The information about the three retrieved scattering parameters CWP, CTH, and APS can nearly entirely be attributed to the O_2 fit window. Scattering properties are defined within the state vector solely by these three parameters. The whole micro physical cloud and aerosol properties like phase function, extinction, and absorption coefficients are only defined in the parameter vector. Unfortunately, these micro physical properties are not known and also not constant in reality and the values that we define in the parameter vector are obviously only a rough estimate.

Let us first consider only the O_2 fit window and assume that extinction and absorption coefficients as well as phase function of the scattering particles are constant in this spectral region. Let us now assume two clouds having phase functions which differ only by a factor (or an offset within a logarithmic plot) outside the forward peak. In such case, the CWP retrieval would be ambiguous in respect to the micro physical properties and consequently, correct CWP values are only retrievable if the scattering particles are known. Referring to Fig. 3, the volume scattering functions within the O_2 fit window of e.g. fractal ice crystals of different size show such similarities. This means that in the case of unknown particles, it is hardly possible to retrieve the true CWP from measurements in the O_2 fit window only. The retrieved CWP is than rather an effective CWP under the assumption of specific particles. Its value does not have to correspond to the true CWP. Note: The same applies to APS and also to some extend to CTH. As long as the true geometrical thickness is known and defined in the parameter vector, the retrieved CTH corresponds to the true CTH. Nevertheless, in reality the true cloud geometrical thickness is unknown and therefore, only an effective CTH can be retrieved under the assumption of a cloud with 0.5 km geometrical thickness. This corresponds to the CTH results of the "CGT" scenario in Table 2.

However, the effective scattering parameters are mainly retrieved from the O_2 fit window without knowledge of the actual micro physical properties. Therefore, the retrieved parameters may not be appropriative for the usage in the CO_2 fit window under some conditions. Particularly, this depends on the relation of the absorption coefficients and volume scattering functions within the O_2 fit window compared to the CO_2 fit window. We can expect that the retrieved parameters are applicable if this relation is similar for the true particles and those particles that we assume within the parameter vector.

Assuming here a static relation is only a rough estimate, because methods like that of Nakajima and King (1990) are based on the fact that liquid water droplets have a stronger absorption at e.g. 1600 nm compared to e.g. 750 nm with nearly no absorption. This results in differences of the reflection at clouds in both wavelengths which can be used to derive the cloud optical thickness and simultaneously the particle's effective radius. However, this method may fail for very thin clouds under conditions with unknown spectral albedo. Additionally, ice particles usually have non-spherical shapes influencing the corresponding phase functions. For these reasons, we did not consider to retrieve the cloud particle effective radius simultaneously.

The clouds we use for the scenarios of this section, consist of fractal ice particles with 100 and 300 µm effective radius ("ice frac. 100" and "ice frac. 300" scenario), hexagonal ice particles with 25 and 50 µm effective radius ("ice hex. 25" and "ice hex. 50" scenario), and water droplets with a gamma particle size distribution and an effective radius of 6, 12, and 18 µm, respectively ("water 6", "water 12", and "water 18" scenario). These scenarios are based on the "met. 1σ" reference scenario. The corresponding volume scattering functions are given in Fig. 3.

For the most common shapes of cloud particles, a decreasing particle size results in an increasing optical thickness and a decreasing forward peak of the phase function. For this reason we use different true CWP values for these scenarios: $3\,g/m^2$ for the "water" scenarios, $8\,g/m^2$ for the "ice hex." scenarios, and $15\,g/m^2$ for the "ice frac." scenarios. Additionally we use different CTH values: 3 km for the "water" scenarios and 15 km, otherwise. The corresponding cloud optical thicknesses (at 500 nm) are 0.25 ("ice frac. 100"), 0.08 ("ice frac. 300"), 0.52 ("ice hex. 25"), 0.29 ("ice hex. 50"), 0.80 ("water 6"), 0.39 ("water 12"), and 0.26 ("water 18").

The SNR values in the O_2 fit window confirm, that more radiation is scattered back from smaller particles. However, all values are in the rage of 1541 and 1614. Compared to this, there is a relative large gap within the CO_2 SNR values between the ice and water scenarios. This is caused by strong absorption of ice in this spectral region which is often used for the retrieval of the cloud thermodynamic phase. This gap, however, indicates that statically defining all micro physical cloud properties in the parameter vector must result in some misinterpretations. In these cases, the enhanced or reduced back scattered radiation is mainly misinterpreted as albedo effect. Given a true albedo of 0.20 within both fit windows, the retrieved albedo varies between 0.20 and 0.22 within the O_2 fit window and 0.20 and 0.23 within the CO_2 fit window. For the retrieved surface pressure, we find systematic errors which are similar to the reference scenario.

The CWP behaves for ice particles as expected and shows negative biases for particles larger than 50 µm and a positive bias, otherwise. The results for water droplets are not so clear. Due to more pronounced differences in the shape of the volume scattering functions and absorption coefficients, we find for these scenarios increased RMS values of the resulting residuals. This especially applies to the O_2 fit window of the "water 12" scenario with a RMS value of 0.28‰. The corresponding expected RMS value due to SNR is about 0.64‰.

For CTH, we find moderate negative biases for the analyzed ice particles which are comparable to the bias of the reference scenario. Only the "ice frac. 300" scenario produces a larger negative bias whereas the corresponding stochastic error hints at a lower sensitivity due to the reduced optical thickness of this cloud. For the water cloud scenarios, we find large systematic biases of the CTH of up to 5.9 km. These may be explained by a rather low true CTH of 3 km being far away from the a priori value of 10 km. Additionally, the profile of the aerosol extinction coefficient has its maximum values in the boundary layer so that misinterpretations with APS may be possible here. Large systematic and stochastic errors are found for APS, showing that the APS retrieval is mainly driven by the a priori information but also hinting that APS may easily be misinterpreted as CTH or CWP.

The systematic errors of the retrieved XCO_2 are in the range of -7.6 and -0.9 ppm for 20° SZA, -5.4 and 0.8 ppm for 40° SZA, and -5.0 and 8.3 ppm for 60° SZA. The corresponding differences to the reference scenario are in the range of -4.4 and 2.3 ppm for 20° SZA, -3.0 and 3.2 ppm for 40° SZA, and -3.8 and 9.5 ppm for 60° SZA. The increased errors at larger solar zenith angles can also be interpreted as errors due to enhanced cloud optical thickness. With increasing SZA, the light path through the cloud and therefore also the apparent optical thickness of the cloud enhances. Vice versa, smaller systematic errors, which are closer to those of the reference scenario, may be expected for lower CWP values.

4.8 Aerosols

Analogous to the cloud scenarios, we estimated the influence of aerosol properties which are not part of the state vector. For this purpose, we confront the algorithm with four aerosol scenarios which are described in detail by Schneising et al. (2008). Their profile, class of particles, and their phase function differ from the default aerosol scenario. The "OPAC background" scenario consists of continental

relatively clean aerosol in the boundary layer and the free troposphere. Its total aerosol optical thickness is 0.099 at 750 nm and 0.026 at 1550 nm. The "OPAC urban" scenario has continental polluted aerosol in the boundary layer and continental average aerosol in the free troposphere. Its total aerosol optical thickness is 0.196 at 750 nm and 0.066 at 1550 nm. The "OPAC desert" scenario consists of desert aerosol in the boundary layer and the continental clean aerosol type in the free troposphere. Its total aerosol optical thickness is 0.264 at 750 nm and 0.188 at 1550 nm. The "extreme in BL" scenario has strongly enhanced urban aerosol in the boundary layer with a visibility of only 2 km and relative humidity of 99%. Its total aerosol optical thickness is 2.528 at 750 nm and 1.056 at 1550 nm. We used the "no cloud" scenario as basis for all aerosol scenarios. Except for the extreme scenario, all result are very similar to those of the "no cloud" reference scenario and the systematic absolute XCO_2 errors are below 0.6 ppm. In contrast to this, the extreme scenario produces much larger systematic errors which are in the range of 2.9 ppm for 20° SZA and 13.9 ppm for 60° SZA.

Schneising et al. (2008) performed a similar error estimation but under slightly different conditions: They used a SZA of 50° and an albedo of 0.1 and found systematic XCO_2 errors of −3.8, −2.5, 1.3, and 21.7 ppm for the "OPAC background", "OPAC urban", "OPAC desert", and the "extreme in BL" scenario, respectively. Under these conditions, we find systematic XCO_2 errors of −0.6, −0.5, −0.6, and 10.6 ppm.

4.9 Column averaging kernel

The averaging kernel matrix gives the sensitivity of the retrieval to the true state. Analogous to this, we define the column averaging kernel vector $\boldsymbol{a}_{CO_2}$ as sensitivity of the retrieved XCO_2 to the true layered CO_2 mixing ratios. In the ideal case all n_{CO_2} elements of $\boldsymbol{a}_{CO_2}$ would be equal 1. This would mean that a XCO_2 change introduced by a change of the ith layer is one-to-one reproduced by the retrieved XCO_2. Considering only those state vector elements i corresponding to the CO_2 profile, the elements of the column averaging kernel vector can be calculated analogous to Connor et al. (2008) by:

$$(\boldsymbol{a}_{CO_2})_i = \frac{\partial \mathrm{XCO_2}}{\partial \boldsymbol{x}_i} \frac{1}{\boldsymbol{w}_i} = (\boldsymbol{w}^T \mathbf{A})_i \frac{1}{\boldsymbol{w}_i} \quad (13)$$

Figure 9 shows the column averaging kernels of nine scenarios which differ by the solar zenith angles, albedo, and cloud water/ice path. All nine scenarios are based on the "dry run" scenario. Except for the "alb. ocean" scenario, the retrieval shows a neutral sensitivity with averaging kernel values close to unity within the lower troposphere i.e. within the lowest three atmospheric layers. Within the upper atmosphere, the CO_2 absorption lines become thinner and therefore deeper due to the reduced ambient pressure so that saturation effects

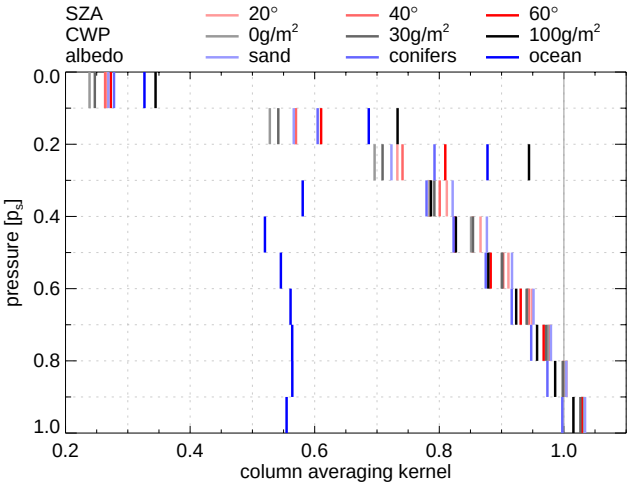

Fig. 9. Column averaging kernels of nine scenarios differing by the solar zenith angles, albedo, and cloud water/ice path. All nine scenarios are based on the "dry run" scenario.

are more pronounced in the line centers. As a result the CO_2 weighting functions show less sensitivity in the upper atmosphere. Additionally, the a priori constraints are much tighter in this region. For these reasons, the averaging kernels of all analyzed cases reduce with height and minimum values between about 0.25 and 0.35 are found in the top layer. This behavior is similar to that found by Connor et al. (2008). Only in the third atmospheric layer between $0.3\,p_s$ and $0.2\,p_s$, a considerable increase is observed for some scenarios. Except for the CWP scenario with 0 g/m^2, all illustrated scenarios have an ice cloud in this layer. This increases the back scattered radiation and therefore also the sensitivity in the layers above the cloud. For bright surfaces, the relative enhancement of radiation can be neglected. In contrast to this, a major part of the detected radiation over dark surfaces is scattered at the cloud layer which increases the sensitivity above the cloud. Accordingly, the effect is more pronounced for thicker clouds, higher solar zenith angles, and lower albedos. If the fraction of backscattered radiation at the cloud layer is low enough, the effect is not observed at all.

4.10 Degree of non-linearity

If the forward model was perfectly linear in all state vector elements, the inversion would always converge within the first iteration. However, in reality the forward model is more or less non-linear in respect to the state vector elements. The degree of non-linearity d_l of a state vector element i can be expressed by evaluating $\delta \boldsymbol{y} = \boldsymbol{F}(\boldsymbol{x}_0', \boldsymbol{b}) - \boldsymbol{F}(\boldsymbol{x}_0, \boldsymbol{b}) - \mathbf{K}(\boldsymbol{x}_0' - \boldsymbol{x}_0)$ which is the difference of $\boldsymbol{F}(\boldsymbol{x}_0', \boldsymbol{b})$ and the linear extrapolation of $\boldsymbol{F}(\boldsymbol{x}_0, \boldsymbol{b})$. Whereas, $\boldsymbol{x}_0'$ differs from $\boldsymbol{x}_0$ only in the ith element. The difference is typically set to one standard

Table 4. Degree of non-linearity of selected state vector elements calculated for the "dry run" reference scenario. Given are the name of the state vector element, the absolute deviation from the reference state vector, the degree of non-linearity, and the absolute XCO_2 error when using a linear instead of the iterative retrieval.

Name	$\lvert\delta x_i\rvert$	d_l	$\lvert\delta XCO_2\rvert$ [ppm]
Albedo P_0 (O_2)	0.05	1.63	0.3
Albedo P_0 (CO_2)	0.05	0.37	0.2
$\Delta\lambda$ (O_2) [nm]	0.10	11.70	13.3
$\Delta\lambda$ (CO_2) [nm]	0.10	0.01	0.0
FWHM (O_2) [nm]	0.10	5.79	6.2
FWHM (CO_2) [nm]	0.10	0.02	0.0
ΔT [K]	1.1	0.97	0.0
H_2O [‰]	0.71	0.01	0.0
APS	1.0	1.44	0.0
CWP [g/m^2]	10.0	16.20	0.0
CTH [km]	5.0	5.17	2.1
p_s [hPa]	31	2.06	0.8
XCO_2 [ppm]	20.9	0.03	0.0

deviation. $\delta\boldsymbol{y}$ is than compared to the measurement error:

$$d_l = \sqrt{\delta\boldsymbol{y}^T \mathbf{S}_\epsilon^{-1} \delta\boldsymbol{y} \frac{1}{m}} \tag{14}$$

This quantity is larger than unity if the spectral error due to linearization exceeds the measurement error and smaller than unity, otherwise. Nevertheless, large values of d_l does not necessarily have to result in large errors of the retrieved XCO_2 because the spectral residual due to linearization does not have to correlate with any other weighting function. On the basis of Eq. (5.1) of Rodgers (2000), the error of the retrieved state vector due to non-linearity $\delta\boldsymbol{x}$ when using a linear retrieval instead of the iterative retrieval is about:

$$\delta\boldsymbol{x} = \mathbf{G}[\boldsymbol{F}(\hat{\boldsymbol{x}}, \boldsymbol{b}) - \boldsymbol{F}(\boldsymbol{x}_0, \boldsymbol{b}) - \mathbf{K}(\hat{\boldsymbol{x}} - \boldsymbol{x}_0)] \tag{15}$$

Analogous to Eq. (11) the corresponding XCO_2 error is:

$$\delta XCO_2 = \boldsymbol{w}^T \delta\boldsymbol{x} \tag{16}$$

As an example, we calculated d_l as well as δXCO_2 for selected state vector elements for the "dry run" scenario at a SZA of 40°. The results are given in Table 4. Most of the analyzed state vector elements result in XCO_2 errors less than 1 ppm which is much smaller than the stochastic error of 3.2 ppm (Table 2).

Several of the analyzed parameters have a degree of non-linearity greater than one but show only minor linearization errors for XCO_2. This especially applies to CWP with d_l=16.20 and $|\delta XCO_2|$=0.0. The largest XCO_2 linearization errors are observed for the non-atmospheric state vector elements of the O_2 fit window: For the slit function's FWHM and for the wavelength shift the XCO_2 error amounts to 6.2 and 13.3 ppm, respectively. However, the test interval of 0.1 nm is very large. For this reason, shift and squeeze of the wavelength axis is iteratively fitted in the WFM-DOAS 1.0 retrieval, whereas linearity is assumed for all other fit parameters. The largest XCO_2 linearization errors of atmospheric parameters would occur when assuming linearity in respect to surface pressure (0.8 ppm), and CTH (2.1 ppm). This accords with Fig. 2 from which influences due to non-linearities of CTH were expected.

However, linearization errors in respect to CTH may be reduced when fitting cloud top pressure instead of CTH. This could reduce the number of needed iterations of an iterative retrieval or reduce the errors of a non-iterative one-step retrieval. In respect to the atmospheric gases H_2O and CO_2 the retrieval is very linear within the a priori uncertainty even though the retrieval uses the sun-normalized radiance but not its logarithm as input for the measurement vector. Note: We here analyze only one specific scenario and non-linearities may be different under other conditions.

5 Conclusions

An optimal estimation based XCO_2 retrieval scheme for measurements in the O_2-A band and in the weak CO_2 absorption band at 1580 nm has been presented. Its error characteristics have been analyzed for a SCIAMACHY like nadir looking satellite instrument with moderate spectral resolution. The proposed method is, however, not restricted to SCIAMACHY measurements and could be adapted to other viewing geometries and spectral characteristics e.g. those of an upward looking ground-based NIR spectrometer. We showed that the retrieval of three scattering parameters from two merged fit windows consisting of measurements in the O_2 and CO_2 band has the potential to drastically reduce systematic XCO_2 errors compared to a WFM-DOAS like retrieval scheme which considers scattering only implicitly. The information about these parameters comes mainly from the O_2 measurements and is made available in the CO_2 band by the merged fit windows approach. The retrieved scattering parameters were: (effective) cloud water/ice path, (effective) cloud top height, and scaling factor for a default aerosol profile.

We found that only minor information is obtainable about the scaling of the aerosol profile with error reductions of about 32%. However, in respect to a planned application to real data, this state vector element enables us to use potential prior knowledge about this parameter without disregarding the available information.

Findings of Schneising et al. (2008) hinted that sub visible cirrus clouds are the major source of error of the WFM-DOAS 1.0 retrieval scheme. For this reason, we focused our analysis on optically thin ice clouds. The error reduction of the cloud parameters was much higher and amounted to over 90% in most of the analyzed scenarios. We explained this with the fact that most of the analyzed clouds had a rather

large cloud top height of 10 km or more which is typical for cirrus clouds. In this height, the spectral properties of oxygen can be distinguished from those near the surface within the simulated SCIAMACHY measurements.

The precision of the retrieved XCO_2 was between 3 and 4 ppm for most of the analyzed scenarios which is smaller but similar to the 1–2% precision range experimentally determined for the WFM-DOAS 1.0 retrieval scheme (Schneising et al., 2008). Slightly lower values were observed for scenarios with high albedo and therefore large signal to noise values. Much larger stochastic errors of up to 12.3 ppm were observed for low albedos of snow or open ocean.

The accuracy for scenes with optically thin cirrus clouds was drastically enhanced compared to a WFM-DOAS like retrieval. At solar zenith angles of 40°, the presence of ice clouds with optical thicknesses in the range of 0.01 to 1.00 contributed with less than 0.5 ppm to the systematic absolute XCO_2 error if a perfect forward model is assumed. This compares to systematic XCO_2 errors of a WFM-DOAS like retrieval scheme in the range of 3 ppm to more than 400 ppm. However, the WFM-DOAS 1.0 processing chain efficiently filters cloud contaminated scenes so that such large errors do not occur in the WFM-DOAS data product.

For scenarios with known parameter vector and with un-modified CO_2 profile ("dry run", "spectral albedo", "no cloud", "CWP", and "CTH"), the systematic XCO_2 errors were most times less than ± 0.5 ppm and always in the range of -1.0 and 0.6 ppm. XCO_2 was systematically underestimated at scenarios with enhanced CO_2 mixing ratio profiles (e.g. "plus 1σ", "plus 3σ", and "art. profile"). The underestimation was interpreted as CO_2 profile smoothing error which results from lower sensitivities and lower a priori uncertainties in respect to the CO_2 mixing ratios in the upper atmosphere. The largest underestimation amounted to -5.7 ppm and occurred for the "plus 3σ" scenario having a considerably enhanced XCO_2 of 439.4 ppm. This value differed from the a priori value by three times of the a priori uncertainty which showed us that the XCO_2 retrieval is dominated by the measurement but not by the a priori. Typical uncertainty reductions of XCO_2 were 78%.

Scattering in clouds was described by only two elements of the state vector. For this reason, the retrieval's sensitivity to other scattering relevant (not retrieved) parameter vector elements has been analyzed. These were micro physical cloud properties like particle size, shape, and state of aggregation resulting in different phase functions, extinction, and absorption coefficients. Due to more similar phase functions, the retrieval performed better and with smaller residuals for ice clouds than for water clouds although lower CWP values have been used for the water clouds. The systematic XCO_2 errors of the "micro physical cloud properties" scenarios with ice clouds were most times below ± 4 ppm. However, for water clouds and for some ice cloud scenarios with 60° solar zenith angle, larger systematic errors of up to 8.3 ppm were observed. In respect to (not retrieved) macro physical cloud properties, we analyzed the retrieval's sensitivity to multilayer clouds, cloud geometrical thickness, and cloud fractional coverage. These properties contributed with -2.8 to 0.9 ppm to the systematic XCO_2 error. The largest effect was observed for the cloud fractional coverage.

Except for the "spectral albedo" scenarios, all scenarios were calculated for a spectrally constant Lambertian albedo of 0.2. However, all calculations were repeated with an albedo of 0.1 and 0.3, respectively. As all scenarios had a semi transparent atmosphere, the albedo strongly influenced the signal to noise ratios. As a result, the stochastic errors were generally higher for an albedo of 0.1 and lower for an albedo of 0.3. Additionally, a dependency of the biases on the surface albedo could be observed. The differences were largest (up to 12 ppm) for the "micro physical cloud properties" scenarios. Otherwise, only minor differences (for most scenarios below 1 ppm) were observed. For the majority of scenarios, the absolute values of the biases were reduced with increasing albedo.

The column averaging kernels of the proposed method had their maximum with values about 1.0 (except for one case) at the surface layer. Higher in the atmosphere, a decreasing sensitivity was observed. Solely, above clouds that significantly contribute to the total backscattered radiation, we observed a local maximum within the averaging kernels. Compared to this, the averaging kernels of XCO_2 retrieval schemes for TIR atmospheric sounders have their maximum in the higher atmosphere at around 210 hPa (Crevoisier et al., 2009). The optimal estimation technique could be utilized to use TIR based CO_2 retrievals as a prior knowledge which would further constrain the CO_2 profile for pressure levels where NIR sensors have only a reduced sensitivity. This is affirmed by Christi and Stephens (2004) who found that TIR and NIR measurements complement one another in retrieving the CO_2 column.

The results presented here indicate that it is theoretically possible to retrieve XCO_2 from SCIAMACHY nadir measurements with an accuracy and precision of about 1% in many cases even in the presence of thin ice clouds. This represents an important step forward for the improvement of XCO_2 retrieval schemes for SCIAMACHY for the following reasons: 1) Most cloud detection schemes are not able to detect sub visible cirrus clouds. 2) Rigorous masking of clouds with optical thicknesses as small as 0.1 or lower would drastically reduce the amount of available data. 3) Large satellite pixels with sizes of 30 times 60 km have a high probability for being cloud contaminated.

Using SCIATRAN as forward model makes the retrieval flexible but computational expensive. This hampers the application to large data amounts produced by SCIAMACHY. Therefore, investigations are ongoing to develop a lookup table approach based on pre calculated radiances which enhances the computational efficiency at acceptable influences on accuracy and precision.

Appendix A

Table A1. As Table 2 but with an spectrally constant albedo of 0.1.

Scenario	SNR		RMS [‰]		SZA 40°					SZA 20°	SZA 60°
	O_2	CO_2	O_2	CO_2	p_s [hPa]	CWP [g/m^2]	CTH [km]	APS	XCO_2 [ppm]	XCO_2 [ppm]	XCO_2 [ppm]
dry run ❍	1108	717	0.01	0.00	0±10	−0.1±1.0	0.0±0.4	0.0±0.6	0.1±4.2	0.1±4.0	−0.0±5.2
met. 1σ ❍	1247	718	0.06	0.13	5±8	0.6±0.7	−0.3±0.4	−0.6±0.6	−2.5±4.6	−3.2±4.4	−1.9±6.7
calibration ♣,❑	1185	770	0.02	0.01	−4±10	1.1±1.0	0.0±0.4	−0.0±0.6	1.2±4.1	1.2±3.9	1.1±4.9
CO_2 profile											
plus 1σ ♣,❍	1108	716	0.03	0.09	1±10	0.1±1.0	−0.0±0.4	−0.0±0.6	−2.3±4.5	−2.1±4.4	−2.8±5.5
plus 3σ ♣,❍	1108	714	0.09	0.28	8±10	0.8±1.0	−0.3±0.4	−0.4±0.6	−7.5±5.4	−7.4±5.4	−9.9±6.1
art. profile ♣,❍	1108	716	0.02	0.07	0±10	0.0±1.0	−0.0±0.4	0.0±0.6	−1.7±4.4	−1.6±4.3	−2.1±5.4
Spectral albedo											
no cloud ♣,❍	981	736	0.03	0.01	−1±3	0.0±0.8	10.0±5.0	−0.0±0.7	−0.3±3.9	−0.4±3.8	−0.2±4.4
CWP 0.3 ♣,❍	984	735	0.02	0.01	0±4	0.1±0.9	−0.1±4.7	−0.0±0.7	−0.3±3.9	−0.4±3.8	−0.1±4.5
CWP 3.0 ♣,❍	1015	728	0.02	0.00	0±8	0.0±1.3	−0.0±1.4	−0.0±0.7	−0.2±4.1	−0.2±3.9	−0.1±4.8
CWP 30.0 ♣,❍	1409	715	0.02	0.02	−5±10	−0.2±0.7	0.0±0.1	0.1±0.6	−0.3±5.2	0.6±4.7	0.5±6.7
CTH 3 ♣,❍	1086	716	0.24	0.02	−9±7	−7.9±1.9	1.8±2.8	0.0±0.9	0.0±4.1	−0.4±4.0	0.4±4.5
CTH 6 ♣,❍	1095	717	0.05	0.00	−2±12	−0.4±2.1	0.1±0.6	−0.0±0.8	0.4±4.4	0.5±4.1	0.7±5.7
CTH 12 ♣,❍	1113	717	0.01	0.00	0±9	−0.0±0.8	−0.0±0.5	0.0±0.6	0.1±4.1	0.1±3.9	−0.0±5.3
CTH 21 ♣,❍	1126	718	0.08	0.00	1±3	0.1±0.3	−0.5±1.1	−0.0±0.4	−0.2±4.1	−0.4±3.8	0.1±5.2
CFC 50 ♦,❑	1137	728	0.07	0.11	0±8	−5.7±0.8	−0.8±0.7	−1.1±0.6	−2.6±4.4	−4.2±4.3	3.5±5.7
CGT ♦,❑	1242	718	0.07	0.13	5±8	0.5±0.7	−1.7±0.3	−0.5±0.7	−2.8±4.6	−3.4±4.3	−2.9±6.7
multilayer ♦,❑	1226	718	0.14	0.13	−3±8	−1.4±1.0	0.2±0.3	−0.2±0.7	−2.2±4.6	−3.0±4.3	−4.1±6.8
Micro physical cloud properties											
ice frac. 100 ♦,❑	1138	718	0.09	0.16	7±8	−5.8±0.8	−0.8±0.7	−0.8±0.7	3.2±4.4	0.2±4.3	13.6±6.6
ice frac. 300 ♦,❑	1057	728	0.11	0.13	7±7	−10.8±1.0	−2.3±1.3	−1.0±0.7	−0.3±4.3	−2.1±4.2	7.0±5.5
ice hex. 25 ♦,❑	1202	744	0.08	0.12	6±8	4.9±0.7	−0.3±0.5	−0.7±0.6	1.7±4.5	−1.3±4.6	6.8±6.5
ice hex. 50 ♦,❑	1140	716	0.09	0.19	2±8	1.5±0.8	−0.6±0.7	−0.9±0.6	6.9±4.5	6.5±4.7	16.4±6.6
water 6 ♦,❑	1196	912	0.19	0.09	−8±9	2.2±2.1	3.5±1.1	−1.5±0.8	−11.9±4.2	−13.0±4.0	−9.4±4.3
water 12 ♦,❑	1102	822	0.47	0.09	−5±6	−1.8±1.1	8.6±3.1	−1.3±0.7	−6.5±4.1	−4.8±4.3	−1.5±4.9
water 18 ♦,❑	1073	793	0.19	0.08	0±8	−0.8±1.6	5.3±2.2	−1.2±0.8	−7.2±4.3	−3.8±4.2	0.1±4.9
Aerosol											
OPAC background ♥,❑	974	737	0.04	0.01	−1±3	0.0±0.7	10.0±5.0	−0.2±0.7	−0.4±3.9	−0.2±3.9	−0.7±4.4
OPAC urban ♥,❑	962	727	0.06	0.00	0±3	−0.0±0.7	10.0±5.0	−0.2±0.7	−0.3±3.9	−0.2±3.8	−0.2±4.4
OPAC desert ♥,❑	1003	757	0.11	0.01	3±4	−0.2±1.0	9.9±5.0	0.2±0.8	0.5±3.9	0.6±3.9	0.2±4.2
extreme in BL ♥,❑	1402	808	0.17	0.05	−20±5	1.3±1.8	5.7±3.4	0.1±0.9	7.7±3.9	4.2±3.9	13.7±3.8

Table A2. As Table 2 but with an spectrally constant albedo of 0.3.

Scenario	SNR		RMS [‰]		SZA 40°					SZA 20°	SZA 60°
	O_2	CO_2	O_2	CO_2	p_s [hPa]	CWP [g/m^2]	CTH [km]	APS	XCO_2 [ppm]	XCO_2 [ppm]	XCO_2 [ppm]
dry run ❍	1935	1437	0.00	0.00	0±5	−0.1±1.0	0.0±0.4	0.0±0.7	0.1±2.9	0.1±2.9	0.0±2.7
met. 1σ ❍	1987	1375	0.05	0.04	3±5	0.5±0.7	−0.3±0.4	−0.6±0.7	−2.4±3.0	−2.7±3.0	−1.4±3.0
calibration ♣,❑	2052	1527	0.07	0.01	−6±5	0.5±0.9	0.4±0.4	−0.1±0.6	0.8±2.8	0.9±2.8	0.8±2.7
CO_2 profile											
plus 1σ ♣,❍	1935	1435	0.03	0.03	0±5	0.0±1.0	0.0±0.4	−0.0±0.6	−1.3±3.2	−1.2±3.2	−1.3±2.9
plus 3σ ♣,❍	1935	1430	0.08	0.10	3±5	0.6±1.0	−0.1±0.4	−0.4±0.6	−5.0±4.0	−4.8±3.9	−4.4±3.4
art. profile ♣,❍	1935	1435	0.03	0.03	0±5	−0.0±1.0	0.0±0.4	0.0±0.7	−1.0±3.1	−0.9±3.1	−1.1±2.8
Spectral albedo											
no cloud ♣,❍	1900	1553	0.03	0.01	−1±4	0.0±0.8	10.0±5.0	−0.0±0.6	−0.4±3.4	−0.0±3.9	−0.4±2.8
CWP 0.3 ♣,❍	1900	1550	0.03	0.01	0±4	0.1±0.9	0.0±4.6	−0.0±0.6	−0.5±3.4	−0.5±3.7	−0.4±2.9
CWP 3.0 ♣,❍	1907	1518	0.03	0.00	0±5	−0.0±1.2	0.1±1.4	0.0±0.7	−0.1±3.3	−0.2±3.4	−0.2±2.9
CWP 30.0 ♣,❍	2064	1240	0.02	0.01	−1±5	−0.2±0.7	0.0±0.1	0.2±0.6	0.2±2.8	0.2±2.7	−0.0±3.2
CTH 3 ♣,❍	1922	1437	0.15	0.02	4±5	−7.9±1.8	2.8±3.3	−0.1±0.8	−1.1±3.7	−1.3±3.7	−0.1±3.1
CTH 6 ♣,❍	1926	1437	0.05	0.00	−1±5	−0.7±2.0	0.2±0.8	0.0±0.8	0.2±3.0	0.1±3.1	0.2±2.8
CTH 12 ♣,❍	1939	1437	0.01	0.00	0±5	−0.0±0.8	0.0±0.4	0.0±0.6	0.1±2.8	0.1±2.9	−0.2±2.7
CTH 21 ♣,❍	1949	1437	0.07	0.00	0±3	0.1±0.3	−0.7±1.2	−0.0±0.4	−0.1±2.5	−0.0±2.5	−0.1±2.7
CFC 50 ♦,❑	1946	1461	0.14	0.04	−1±5	−6.2±0.8	−0.2±0.9	−1.1±0.6	−6.0±3.2	−6.1±3.2	−2.2±3.0
CGT ♦,❑	1983	1374	0.04	0.04	4±5	0.5±0.7	−1.7±0.3	−0.6±0.7	−2.5±3.0	−2.8±3.0	−1.5±3.0
multilayer ♦,❑	1970	1374	0.13	0.04	2±4	−1.4±0.9	0.3±0.3	−0.3±0.7	−2.2±2.9	−2.5±3.0	−1.4±3.1
Micro physical cloud properties											
ice frac. 100 ♦,❑	1942	1452	0.05	0.03	5±5	−5.9±0.8	−0.6±0.7	−0.8±0.7	−3.4±3.1	−4.4±3.2	2.6±2.8
ice frac. 300 ♦,❑	1914	1511	0.07	0.03	6±5	−11.0±1.0	−1.9±1.3	−0.9±0.7	−4.4±3.4	−5.2±3.5	−0.2±3.0
ice hex. 25 ♦,❑	1965	1455	0.06	0.04	5±5	5.0±0.7	−0.4±0.5	−0.7±0.7	−1.2±3.1	−2.8±3.0	2.5±2.9
ice hex. 50 ♦,❑	1940	1448	0.05	0.04	3±5	1.5±0.8	−0.6±0.7	−1.0±0.7	−1.7±3.2	−2.4±3.1	4.4±2.9
water 6 ♦,❑	1968	1591	0.21	0.11	2±5	−0.5±1.8	4.6±1.8	−0.6±0.8	−0.9±4.0	−3.1±3.9	−2.9±3.2
water 12 ♦,❑	1936	1571	0.13	0.04	5±5	−1.0±1.6	5.5±2.0	−1.0±0.8	−3.8±4.1	−2.4±4.0	−0.7±3.3
water 18 ♦,❑	1924	1561	0.11	0.04	6±5	−0.9±1.7	5.1±1.9	−1.0±0.8	−4.6±4.1	−3.2±4.0	−1.1±3.3
Aerosol											
OPAC background ♥,❑	1903	1557	0.02	0.01	−1±4	0.0±0.8	10.1±5.0	−0.2±0.6	−0.1±3.4	0.9±3.9	−0.5±2.7
OPAC urban ♥,❑	962	727	0.06	0.00	0±3	−0.0±0.7	10.0±5.0	−0.2±0.7	−0.3±3.9	−0.2±3.8	−0.2±4.4
OPAC desert ♥,❑	1883	1557	0.05	0.01	2±4	−0.2±0.8	10.0±5.0	0.1±0.6	2.1±3.5	2.1±3.9	2.1±2.9
extreme in BL ♥,❑	1807	1420	0.17	0.04	−5±4	0.0±1.1	9.3±4.8	0.5±0.8	5.8±3.7	2.0±3.7	13.0±3.5

Acknowledgements. This study was funded by DLR-Bonn (grant 50EE0507), ESA (ADVANSE project), the EU (FP7 MACC and CityZen), and the State and the University of Bremen, Germany. We thank NOAA for making available the CarbonTracker CO_2 fields and the radiosonde data. We thank ECMWF for providing the meteorological data. We further thank our reviewers for their helpful and valuable comments to improve this work. Many thanks are given to S. Pfeifer and J. Reuter for proofreading the manuscript.

Edited by: G. Stiller

References

Aben, I., Hasekamp, O., and Hartmann, W.: Uncertainties in the space-based measurements of CO_2 columns due to scattering in the Earth's atmosphere, J. Quant. Spectrosc. Radiat. Transfer, 104, 450–459, doi:10.1016/j.jqsrt.2006.09.013, 2007.

Aumann, H. H., Gregorich, D., and Gaiser, S.: AIRS hyperspectral measurements for climate research: Carbon dioxide and nitrous oxide effects, Geophys. Res. Lett., 32, L05806, doi:10.1029/2004GL021784, 2005.

Barkley, M. P., Frieß, U., and Monks, P. S.: Measuring atmospheric CO_2 from space using Full Spectral Initiation (FSI) WFM-DOAS, Atmos. Chem. Phys., 6, 3517–3534, 2006a, http://www.atmos-chem-phys.net/6/3517/2006/.

Barkley, M. P., Monks, P. S., and Engelen, R. J.: Comparison of SCIAMACHY and AIRS CO_2 measurements over North America during the summer and autumn of 2003, Geophys. Res. Lett., 33, L20805, doi:10.1029/2006GL026807, 2006b.

Barkley, M. P., Monks, P. S., Frieß, U., Mittermeier, R. L., Fast, H., Körner, S., and Heimann, M.: Comparisons between SCIAMACHY atmospheric CO_2 retrieved using (FSI) WFM-DOAS to ground based FTIR data and the TM3 chemistry transport model, Atmos. Chem. Phys., 6, 4483–4498, 2006c, http://www.atmos-chem-phys.net/6/4483/2006/.

Barkley, M. P., Monks, P. S., Hewitt, A. J., Machida, T., Desai, A., Vinnichenko, N., Nakazawa, T., Yu Arshinov, M., Fedoseev, N., and Watai, T.: Assessing the near surface sensitivity of SCIAMACHY atmospheric CO_2 retrieved using (FSI) WFM-DOAS, Atmos. Chem. Phys., 7, 3597–3619, 2007, http://www.atmos-chem-phys.net/7/3597/2007/.

Bösch, H., Toon, G. C., Sen, B., Washenfelder, R. A., Wennberg, P. O., Buchwitz, M., de Beek, R., Burrows, J. P., Crisp, D., Christi, M., Connor, B. J., Natraj, V., and Yung, Y. L.: Space-based near-infrared CO_2 measurements: Testing the Orbiting Carbon Observatory retrieval algorithm and validation concept using SCIAMACHY observations over Park Falls, Wisconsin, J. Geophys. Res., 111, D23302, doi:10.1029/2006JD007080, 2006.

Bovensmann, H., Burrows, J. P., Buchwitz, M., Frerick, J., Noël, S., Rozanov, V. V., Chance, K. V., and Goede, A.: SCIAMACHY – Mission Objectives and Measurement Modes, J. Atmos. Sci., 56, 127–150, 1999.

Bril, A., Oshchepkov, S., Yokota, T., and Inoue, G.: Parameterization of aerosol and cirrus cloud effects on reflected sunlight spectra measured from space: application of the equivalence theorem, Appl. Opt., 46, 2460–2470, 2007.

Buchwitz, M. and Burrows, J. P.: Retrieval of CH_4, CO, and CO_2 total column amounts from SCIAMACHY near-infrared nadir spectra: Retrieval algorithm and first results, in: Remote Sensing of Clouds and the Atmosphere VIII, edited by: Schäfer, K. P., Comèron, A., Carleer, M. R., and Picard, R. H., Proceedings of SPIE, 5235, 375–388, 2004.

Buchwitz, M., Rozanov, V. V., and Burrows, J. P.: A correlated-k distribution scheme for overlapping gases suitable for retrieval of atmospheric constituents from moderate resolution radiance measurements in the visible/near-infrared spectral region, J. Geophys. Res., 105, 15247–15261, 2000a.

Buchwitz, M., Rozanov, V. V., and Burrows, J. P.: A near-infrared optimized DOAS method for the fast global retrieval of atmospheric CH_4, CO, CO_2, H_2O, and N_2O total column amounts from SCIAMACHY Envisat-1 nadir radiances, J. Geophys. Res., 105, 15231–15245, 2000b.

Buchwitz, M., de Beek, R., Burrows, J. P., Bovensmann, H., Warneke, T., Notholt, J., Meirink, J. F., Goede, A. P. H., Bergamaschi, P., Körner, S., Heimann, M., and Schulz, A.: Atmospheric methane and carbon dioxide from SCIAMACHY satellite data: initial comparison with chemistry and transport models, Atmos. Chem. Phys., 5, 941–962, 2005a, http://www.atmos-chem-phys.net/5/941/2005/.

Buchwitz, M., de Beek, R., Noël, S., Burrows, J. P., Bovensmann, H., Bremer, H., Bergamaschi, P., Körner, S., and Heimann, M.: Carbon monoxide, methane and carbon dioxide columns retrieved from SCIAMACHY by WFM-DOAS: year 2003 initial data set, Atmos. Chem. Phys., 5, 3313–3329, 2005b, http://www.atmos-chem-phys.net/5/3313/2005/.

Chédin, A., Hollingsworth, A., Scott, N. A., Serrar, S., Crevoisier, C., and Armante, R.: Annual and seasonal variations of atmospheric CO_2, N_2O and CO concentrations retrieved from NOAA/TOVS satellite observations, Geophys. Res. Lett., 29, 1269, doi:10.1029/2001GL014082, 2002.

Chédin, A., Serrar, S., Scott, N. A., Crevoisier, C., and Armante, R.: First global measurement of midtropospheric CO_2 from NOAA polar satellites: Tropical zone, J. Geophys. Res., 108, 4581, doi:10.1029/2003JD003439, 2003.

Chevallier, F., Bréon, F.-M., and Rayner, P. J.: Contribution of the Orbiting Carbon Observatory to the estimation of CO_2 sources and sinks: Theoretical study in a variational data assimilation framework, J. Geophys. Res., 112, D09307, doi:10.1029/2006JD007375, 2007.

Christi, M. J. and Stephens, G. L.: Retrieving profiles of atmospheric CO_2 in clear sky and in the presence of thin cloud using spectroscopy from the near and thermal infrared: a preliminary case study, J. Geophys. Res., 109, D04316, doi:10.1029/2003JD004058, 2004.

Connor, B. J., Boesch, H., Toon, G., Sen, B., Miller, C., and Crisp, D.: Orbiting carbon observatory: Inverse method and prospective error analysis, J. Geophys. Res.-Atmos., 113, D05305, doi:10.1029/2006JD008336, 2008.

Crevoisier, C., Chedin, A., Matsueda, H., Machida, T., Armante, R., and Scott, N. A.: First year of upper tropospheric integrated content of CO_2 from IASI hyperspectral infrared observations, Atmos. Chem. Phys., 9, 4797–4810, 2009, http://www.atmos-chem-phys.net/9/4797/2009/.

Crisp, D., Atlas, R. M., Bréon, F.-M., Brown, L. R., Burrows, J. P., Ciais, P., Connor, B. J., Doney, S. C., Fung, I. Y., Jacob, D. J., Miller, C. E., O'Brien, D., Pawson, S., Randerson, J. T., Rayner, P., Salawitch, R. S., Sander, S. P., Sen, B., Stephens, G. L., Tans, P. P., Toon, G. C., Wennberg, P. O., Wofsy, S. C., Yung, Y. L., Kuang, Z., Chudasama, B., Sprague, G., Weiss, P., Pollock, R., Kenyon, D., and Schroll, S.: The Orbiting Carbon Observatory (OCO) mission, Adv. Space Res., 34, 700–709, 2004.

Engelen, R. J. and McNally, A. P.: Estimating atmospheric CO_2 from advanced infrared satellite radiances within an operational 4D-Var data assimilation system: Results and validation, J. Geophys. Res., 109, D18305, doi:10.1029/2005JD005982, 2005.

Engelen, R. J., Andersson, E., Chevallier, F., Hollingsworth, A., Matricardi, M., McNally, A. P., Thépaut, J.-N., and Watts, P. D.: Estimating atmospheric CO_2 from advanced infrared satellite radiances within an operational 4D-Var data assimilation system: Methodology and first results, J. Geophys. Res., 109, D19309, doi:10.1029/2004JD004777, 2004.

Houweling, S., Breon, F.-M., Aben, I., Rödenbeck, C., Gloor, M., Heimann, M., and Ciais, P.: Inverse modeling of CO_2 sources and sinks using satellite data: a synthetic inter-comparison of measurement techniques and their performance as a function of space and time, Atmos. Chem. Phys., 4, 523–538, 2004, http://www.atmos-chem-phys.net/4/523/2004/.

Houweling, S., Hartmann, W., Aben, I., Schrijver, H., Skidmore, J., Roelofs, G.-J., and Breon, F.-M.: Evidence of systematic errors in SCIAMACHY-observed CO_2 due to aerosols, Atmos. Chem. Phys., 5, 3003–3013, 2005, http://www.atmos-chem-phys.net/5/3003/2005/.

Kokhanovsky, A. A., von Hoyningen-Huene, W., Rozanov, V. V., Noel, S., Gerilowski, K., Bovensmann, H., Bramstedt, K., Buchwitz, M., and Burrows, J. P.: The semianalytical cloud retrieval algorithm for SCIAMACHY - II. The application to MERIS and SCIAMACHY data, Atmos. Chem. Phys., 6, 4129–4136, 2006, http://www.atmos-chem-phys.net/6/4129/2006/.

Kuang, Z., Margolis, J., Toon, G., Crisp, D., and Yung, Y.: Spaceborne measurements of atmospheric CO_2 by high-resolution NIR spectrometry of reflected sunlight: an introductory study, Geophy. Res. Let., 29, 1716, doi:10.1029/2001GL014298, 2002.

Maddy, E. S., Barnet, C. D., Goldberg, M., Sweeney, C., and Liu, X.: CO_2 retrievals from the Atmospheric Infrared Sounder: Methodology and validation, J. Geophys. Res., 113, D11301, doi:10.1029/2007JD009402, 2008.

Miller, C. E., Crisp, D., DeCola, P. L., Olsen, S. C., Randerson, J. T., Michalak, A. M., Alkhaled, A., Rayner, P., Jacob, D. J., Suntharalingam, P., Jones, D. B. A., Denning, A. S., Nicholls, M. E., Doney, S. C., Pawson, S., Boesch, H., Connor, B. J., Fung, I. Y., O'Brien, D., Salawitch, R. J., Sander, S. P., Sen, B., Tans, P., Toon, G. C., Wennberg, P. O., Wofsy, S. C., Yung, Y. L., and Law, R. M.: Precision requirements for space-based X_{CO_2} data, J. Geophys. Res., 112, D10314, doi:10.1029/2006JD007659, 2007.

Nakajima, T. and King, M. D.: Determination of optical thickness and effective particle radius of clouds from reflected solar radiation measurements. Part I: Theory, J. Atmos. Sci., 47, 1878–1893, 1990.

Nazaryan, H., McCormick, M. P., and Menzel, W. P.: Global characterization of cirrus clouds using CALIPSO data, J. Geophys. Res.-Atmos., 113, D16211, doi:10.1029/2007JD009481, 2008.

Palmer, P. I., and Rayner, P.: Failure to launch, Nature Geosci., 2, 247, doi:10.1038/ngeo495, 2009.

Peters, W., Jacobson, A. R., Sweeney, C., Andrews, A. E., Conway, T. J., Masarie, K., Miller, J. B., Bruhwiler, L. M. P., Pétron, G., Hirsch, A. I., Worthy, D. E. J., van der Werf, G. R., Randerson, J. T., Wennberg, P. O., Krol, M. C., and Tans, P. P.: An atmospheric perspective on North American carbon dioxide exchange: CarbonTracker, Proceedings of the National Academy of Sciences (PNAS) of the United States of America, 27 November 2007, 104, 18925–18930, 2007.

Rayner, P. J. and O'Brien, D. M.: The utility of remotely sensed CO_2 concentration data in surface inversions, Geophys. Res. Lett., 28, 175–178, 2001.

Reuter, M., Thomas, W., Albert, P., Lockhoff, M., Weber, R., Karlsson, K. G., and Fischer, J.: The CM-SAF and FUB cloud detection schemes for SEVIRI: Validation with synoptic data and initial comparison with MODIS and CALIPSO, J. Appl. Met. Clim., 48, 301–316, doi:10.1175/2008JAMC1982.1, 2009.

Rodgers, C. D.: Inverse Methods for Atmospheric Sounding: Theory and Practice, World Scientific Publishing, 2000.

Rodriguez, D. G. L., Thomas, W., Livschitz, Y., Ruppert, T., Albert, P., and Hollmann, R.: Cloud properties derived from GOME/ERS-2 backscatter data for trace gas retrieval, IEEE T. Geosci. Remote., 45, 2747–2758, doi:10.1109/TGRS.2007.901043, 2007.

Rothman, L. S., Gordon, I. E., Barbe, A., Benner, D. C., Bernath, P. E., Birk, M., Boudon, V., Brown, L. R., Campargue, A., Champion, J. P., Chance, K., Coudert, L. H., Dana, V., Devi, V. M., Fally, S., Flaud, J. M., Gamache, R. R., Goldman, A., Jacquemart, D., Kleiner, I., Lacome, N., Lafferty, W. J., Mandin, J. Y., Massie, S. T., Mikhailenko, S. N., Miller, C. E., Moazzen-Ahmadi, N., Naumenko, O. V., Nikitin, A. V., Orphal, J., Perevalov, V. I., Perrin, A., Predoi-Cross, A., Rinsland, C. P., Rotger, M., Simeckova, M., Smith, M. A. H., Sung, K., Tashkun, S. A., Tennyson, J., Toth, R. A., Vandaele, A. C., and Vander Auwera, J.: The HITRAN 2008 molecular spectroscopic database, J. Quant. Spectrosc. Ra., 110, 533–572, doi:10.1016/j.jqsrt.2009.02.013, 2009.

Rozanov, A., Rozanov, V., Buchwitz, M., Kokhanovsky, A., and Burrows, J.: SCIATRAN 2.0 – A new radiative transfer model for geophysical applications in the 175–2400 nm spectral region, in: Atmospheric remote sensing: Earth's surface, troposphere, stratosphere and mesosphere – 1, edited by: Burrows, J. P. and Eichmann, K. U., vol. 36 of Adv. Space Res., 1015–1019, doi:10.1016/j.asr.2005.03.012, 35th COSPAR Scientific Assembly, Paris, France, 18–25 July 2004, 2005.

Schneising, O., Buchwitz, M., Burrows, J. P., Bovensmann, H., Reuter, M., Notholt, J., Macatangay, R., and Warneke, T.: Three years of greenhouse gas column-averaged dry air mole fractions retrieved from satellite – Part 1: Carbon dioxide, Atmos. Chem. Phys., 8, 3827–3853, 2008, http://www.atmos-chem-phys.net/8/3827/2008/.

Stephens, B. B., Gurney, K. R., Tans, P. P., Sweeney, C., Peters, W., Bruhwiler, L., Ciais, P., Ramonet, M., Bousquet, P., Nakazawa, T., Aoki, S., Machida, T., Inoue, G., Vinnichenko, N., Lloyd, J., Jordan, A., Heimann, M., Shibistova, O., Langenfelds, R. L., Steele, L. P., Francey, R. J., and Denning, A. S.: Weak northern and strong tropical land carbon uptake from vertical profiles of atmospheric CO_2, Science, 316, 1732–1735,

doi:10.1126/science.1137004, 2007.

Strow, L. L., Hannon, S. E., De-Souza Machado, S., Motteler, H. E., and Tobin, D. C.: Validation of the Atmospheric Infrared Sounder radiative transfer algorithm, J. Geophys. Res., 111, D09S06, doi:10.1029/2005JD006146, 2006.

van Diedenhoven, B., Hasekamp, O. P., and Landgraf, J.: Retrieval of cloud parameters from satellite-based reflectance measurements in the ultraviolet and the oxygen A-band, J. Geophys. Res.-Atmos., 112, D15208, doi:10.1029/2006JD008155, 2007.

Wang, P., Stammes, P., van der A, R., Pinardi, G., and van Roozendael, M.: FRESCO+: an improved O_2 A-band cloud retrieval algorithm for tropospheric trace gas retrievals, Atmos. Chem. Phys., 8, 6565–6576, 2008, http://www.atmos-chem-phys.net/8/6565/2008/.

Wang, P. H., Minnis, P., McCormick, M. P., Kent, G. S., and Skeens, K. M.: A 6-year climatology of cloud occurrence frequency from stratospheric aerosol and gas experiment II observations (1985–1990), J. Geophys. Res.-Atmos., 101, 29407–29429, 1996.

Winker, D. M. and Trepte, C. R.: Laminar cirrus observed near the tropical tropopause by LITE, Geophys. Res. Lett., 25, 3351–3354, 1998.

Yokota, T., Oguma, H., Morino, I., and Inoue, G.: A nadir looking SWIR sensor to monitor CO_2 column density for Japanese GOSAT project, Proceedings of the twenty-fourth international symposium on space technology and science. Miyazaki: Japan Society for Aeronautical and Space Sciences and ISTS, 887–889, 2004.